

KATSUWONUS PELAMIS:  
A CASE STUDY OF THUNNIFORM PROPULSION

by

MICHA BEN-ZVI  
BSc., The University of Alberta, 2006

A THESIS SUBMITTED IN PARTIAL FULFILLMENT OF  
THE REQUIREMENTS FOR THE DEGREE OF

MASTER OF SCIENCE

in

THE FACULTY OF GRADUATE STUDIES

(Zoology)

THE UNIVERSITY OF BRITISH COLUMBIA

(Vancouver)

July 2011

© Micha Ben-Zvi, 2011

## **Abstract**

Thunniform propulsion is considered a case study in convergent evolution. Independently derived at least four times (whales, lamnid sharks, tunas and ichthyosaurs) it is characterized by uniquely high lift based thrust and efficient performance. As such it has been the focus of a great deal of study from not only biologists but engineers and physicists as well. Unfortunately direct physical measurement of this phenomenon is notoriously difficult to obtain. Therefore the majority of the research on the topic so far has consisted of either theoretical modeling or experimental testing with low bio-fidelity.

The purpose of this study was to create a test apparatus that would more accurately mimic thunniform propulsion as seen in the study organism skipjack tuna (*Katsuwonus pelamis*). Such factors as motion parameters and swimming speeds as well as caudal fin size, shape and material properties were all taken into account and matched with in-vivo measurements. Instantaneous lateral and in-flow force measurements were taken throughout testing over a range of motion regimes.

Overall, general motion parameter requirements for thrust generation were determined and quantified. Thrust production, of up to 0.42 N with a coefficient of thrust of approximately 0.2, was found to be in line with whole body drag estimates at tested conditions. Efficiency measurements however, were found to be extremely low (max of 35%) when compared to estimates in the literature of up to 90%. Quasi-static analysis was also conducted and shown to under-predict true thrust values by approximately 50%. A maximum coefficient of lift value was found to be approximately 0.55 at an angle of attack of 25° using this method.

# **Table of Contents**

<b>ABSTRACT</b> .....	<b>ii</b>
<b>TABLE OF CONTENTS</b> .....	<b>iii</b>
<b>LIST OF TABLES</b> .....	<b>v</b>
<b>LIST OF FIGURES</b> .....	<b>vi</b>
<b>LIST OF SYMBOLS</b> .....	<b>vii</b>
<b>ACKNOWLEDGMENTS</b> .....	<b>viii</b>
<b>DEDICATION</b> .....	<b>ix</b>
<b>INTRODUCTION</b> .....	<b>1</b>
<b>BACKGROUND</b> .....	<b>6</b>
BIOLOGICAL.....	6
ENGINEERING .....	9
<b>METHODS</b> .....	<b>16</b>
CREATING TAIL MODELS .....	16
SPECIMEN SELECTION .....	22
WATER TUNNEL SELECTION AND CALIBRATION.....	23
<i>Selection</i> .....	23
<i>Calibration</i> .....	25
<i>Boundary Layer</i> .....	28
DEFINING MOTION REGIMES .....	28
APPARATUS CONSTRUCTION .....	31
<i>Design Selection</i> .....	31
<i>Design</i> .....	32
<i>Calibration</i> .....	37
DATA COLLECTION /TESTING .....	41
<b>RESULTS/ANALYSIS</b> .....	<b>44</b>
DYNAMIC TESTING RESULTS .....	44
<i>Mean Thrust/Drag Values</i> .....	44
<i>Thrust/Lateral Force Profiles</i> .....	46
<i>Power and Efficiency</i> .....	49
<i>Repeatability</i> .....	50
QUASI-STATIC TESTING .....	51
<i>Coefficient of Lift/Drag</i> .....	51
<i>Mean Thrust Values</i> .....	54
<i>Thrust/Lateral Force Profiles</i> .....	55
SYMMETRY ANALYSIS .....	58
<b>DISCUSSION</b> .....	<b>62</b>
HYPOTHESIS 1 .....	62
HYPOTHESIS 2 .....	66
HYPOTHESIS 3 .....	68
HYPOTHESIS 4 .....	70
HYPOTHESIS 5 .....	72
HYPOTHESIS 6 .....	75
FUTURE DIRECTIONS .....	77
<i>Refined Motion Regimes</i> .....	77
<i>Theoretical Modeling Comparison</i> .....	78

<i>Upgrading 'Da Bruce</i> .....	78
<i>Testing Different Foils</i> .....	80
<i>Testing Assumptions</i> .....	81
CONCLUSION .....	81
<b>REFERENCES .....</b>	<b>83</b>
<b>APPENDIX A- MODEL CREATION INSTRUCTIONS.....</b>	<b>86</b>
<b>APPENDIX B- BOUNDARY LAYER CALCULATIONS .....</b>	<b>87</b>
<b>APPENDIX C- DETAILED RESULTS .....</b>	<b>88</b>

## **List of Tables**

TABLE 1- TEST PARAMETER VALUES.....	31
TABLE 2 - SUMMARY OF RESULTS.....	58
TABLE 3 - LINEAR REGRESSIONS BY PARAMETER.....	71
TABLE 4 - RECOMMENDED TEST PARAMETER RANGES.....	77

## **List of Figures**

FIGURE 1-THUNNIFORM SWIMMERS .....	2
FIGURE 2- SWIMMING UNDULATIONS.....	6
FIGURE 3- THUNNIFORM HYDROFOILS .....	7
FIGURE 4- THUNNIFORM UNDULATIONS.....	8
FIGURE 5-WAKE VISUALIZATION .....	11
FIGURE 6- PITCHING AXIS .....	12
FIGURE 7- FOIL CHARACTERISTICS .....	13
FIGURE 8- PITCH AND ATTACK ANGLE .....	14
FIGURE 9- PHASE LAG.....	15
FIGURE 10- LASER SCANNER .....	18
FIGURE 11- TAIL MODEL .....	19
FIGURE 12- MTS SETUP .....	20
FIGURE 13-MATERIAL PROPERTY COMPARISON.....	21
FIGURE 14- TEST SECTION DIAGRAM .....	25
FIGURE 15- TEST SECTION VELOCITY PROFILE.....	27
FIGURE 16- TEST SECTION CALIBRATION.....	27
FIGURE 17A- 'DA BRUCE' .....	33
FIGURE 17B- 'DA BRUCE' .....	34
FIGURE 18- CAM/SCOTCH YOKE COMPARISON.....	37
FIGURE 19- FORCE DIAGRAM .....	39
FIGURE 20- IN-FLOW CALIBRATION .....	39
FIGURE 21- LATERAL CALIBRATION.....	40
FIGURE 22- LASER CALIBRATION .....	41
FIGURE 23-DATA FILTERING.....	47
FIGURE 24-STANDARDIZED TAIL BEAT.....	48
FIGURE 25- NORMALIZED TAIL BEAT .....	48
FIGURE 26- COEFFICIENTS OF LIFT AND DRAG.....	52
FIGURE 27- POLAR DIAGRAM.....	53
FIGURE 28- QUASI-STATIC ANALYSIS .....	54
FIGURE 29A- BIOLOGICALLY RELEVANT FLOW PROFILES .....	56
FIGURE 29B- BIOLOGICALLY RELEVANT FLOW PROFILES .....	57
FIGURE 30- SYMMETRY ANALYSIS .....	60
FIGURE 31- SYMMETRY COMPARISON .....	60
FIGURE 32- PHASE LAG DIAGRAMS .....	64
FIGURE 33- MEASURED VS. CALCULATED RESULTS .....	70
FIGURE 34- FORCE VS $\theta$ RESULTS.....	72
FIGURE 35- DROSOPHILA FORCE GENERATION .....	74
FIGURE 36- PERFORMANCE COMPARISON .....	76

## List of Symbols

Symbol	Description
$f$	Frequency
$U$	Free Stream Velocity
$A_0$	Maximum Yaw Amplitude
$A$	Instantaneous Yaw Amplitude
$H_0$	Normalized Maximum Yaw Amplitude
$SMC$	Standard Mean Chord Length
$t$	Time
$c$	Chord Length
$S_c$	Planform Area
$\Lambda$	Sweepback Angle
$b$	Span
$\theta$	Instantaneous Pitching Angle
$\theta_0$	Nominal Pitching Angle
$\phi$	Phase Lag
$\alpha$	Instantaneous Angle of Attack
$\alpha_m$	Mean Angle of Attack
$St$	Strouhal Number
$l$	Characteristic Length
$\nu$	Kinematic Viscosity
$\rho$	Density
$D$	Drag
$S$	Surface Area
$C_D$	Coefficient of Drag
$C_L$	Coefficient of Lift
$\eta$	Froude Efficiency
$P_{in}$	Input Power
$P_{in}$	Output Power
$F$	Force
$C_T$	Coefficient of Thrust
$\delta$	Boundary Layer Thickness

## **Acknowledgments**

I would like to acknowledge a number of people for their help during the course of my M.Sc. First and foremost, to my supervisor Bob Shadwick, not many people would have accepted an engineer with no biology background into a comparative physiology program, but for some unknown reason you did. Thanks for all the advice and help throughout the entire process, it's been a great couple of years. Next up, the rest of my thesis committee John Gosline (my grand-supervisor) and Sheldon Green, who were both great resources and without whom this project would have never left the ground. Also a very special thanks to the staff in the biology machine shop and Bruce Gillespie in particular, for your tireless work on my test apparatus. I can't count the number of hours you spend designing, building and adjusting that crazy contraption.

Obviously, there are many other friends and family (far too many to mention entirely) that deserve some credit for all of this. From the Pintos (who housed me when I had nowhere else to go), to the rest of the comparative physiology group (who never got tired of my silly 'first year' questions), all the way to my own family, who were so supportive when I announced I was going to quit my job, move to the west coast and study fish. And obviously Megan, for being so wonderful and supportive these last few years, you've been truly amazing.

## **Dedication**

To my nieces and nephews...

## **Introduction**

The evolution of thrust generation via oscillating and pitching foils has proven to be a repeated theme throughout the animal kingdom. From birds to fish to insects, the same basic phenomenon appears again and again. While this topic has been explored extensively via theoretical models (Parry, 1949; Lighthill, 1970; Chopra, 1974, Chopra and Kambe, 1977; Cheng and Murillo, 1984; Bose and Lien, 1989; etc), physical modeling and testing in this field is relatively new. Yet despite the fact that this line of research has only recently begun, it has already generated a whole suite of unexpected and even paradigm shifting discoveries. While exploring why conventional theoretical modeling failed to predict insect flight capabilities, Dickinson et al., (1999) used scaled models to discover two previously unknown thrust generation mechanisms in insects. Shortly thereafter Videler et al., (2004) used similar methods to not only refine existing models on the flight of swifts, but also discovered previously unidentified localization of function along a swift's wing. Both these studies greatly altered the way their respective animals were studied and modeled. The research proposed below will continue this experimental approach by expanding it to the study of aquatic propulsion in thunniform swimmers.

Thunniform locomotion is of particular interest as it is an evolutionary convergent form of propulsion common in many apex aquatic organisms, such as some lamnid sharks, teleosts and cetaceans (as seen in Figure 1). Primarily characterized by posteriorly confined body undulations in combination with a crescent or lunate shaped tail (as exemplified by the tuna, e.g. *Thunnus sp.*), this form of locomotion is estimated to be capable of producing efficiencies in the range of 80-90% + (Fish et al., 1996; Triantafyllou and Triantafyllou, 1995). It is therefore not surprising that this form of locomotion has been so frequently adopted by large continuous open

water swimmers, and is the subject of much interest from both biological and engineering perspectives.

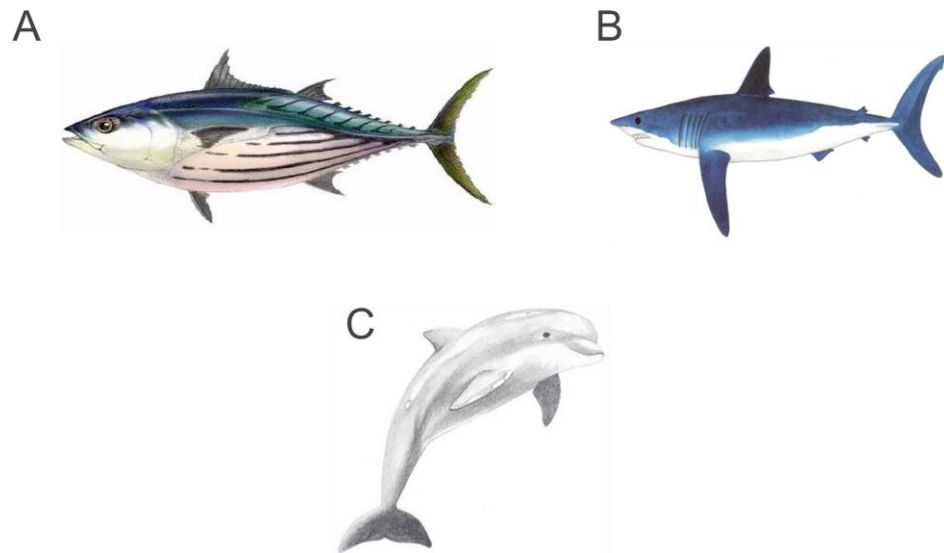


**Figure 1-Thunniform Swimmers:** Examples of three common thunniform swimmers, skipjack tunas (*Katsuwonus pelamis*) (A), shortfin mako sharks (*Isurus oxyrinchus*) (B) and bottlenose dolphins (*Tursiops*) (C). All images modified from [www.vetcraftsportsfishing.com](http://www.vetcraftsportsfishing.com).

Unfortunately, as could be expected when two specialized fields such as engineering and biology overlap, there is often a great deal of confusion and contradictory explanations in the literature regarding thunniform propulsion. Simple points of clarification such as commonly used nomenclatures are often taken for granted. For example the amplitude of an organism's tail beat is often taken at different points depending on whether the individual studying it is an engineer or biologist. Other terms such as lift, drag and thrust, which have been adopted from related work in aeronautics, are often used loosely leading to a great deal of confusion. Typically this is due to the fact that aeronautics deals with a relatively steady state between a foil and its medium. When studying thunniform swimming, the foil motion relative to the medium is not constant, therefore new frames of reference must be created for these terms to have any relevant meaning. Moreover, the very mechanics explaining how thunniform propulsion takes place are often poorly described, or even contradictory. Again, most commonly these issues arise when basic

concepts from aeronautics are loosely applied to thunniform swimming. Often such factors as medium density and viscosity are only addressed on a superficial level, when in fact they can have drastic effects on not only the quantity of thrust generated, but also the very manner in which it is generated.

This project will attempt to address these technical issues as well as the lack of experimental data regarding physically verifiable force generated during thunniform swimming. This will be done by creating a novel test mechanism to imitate both the physical structure and motion of a skipjack tuna (*Katsuwonus pelamis*) tail. Several simplifications will be used in order to generate this ‘first generation’ modeling. To begin with, as it is known that the caudal fin generates a staggering 90% of thunniform propulsion thrust (Fierstine and Walters, 1968), only the region posterior to the peduncle will be modeled. Furthermore as the tail of the skipjack is generally symmetrical (a fact true for most thunniform swimmers), only half of the tail will be modeled. The missing half will be accounted for with the use of a mirror plane in the water along the axis of symmetry. Finally as the true motion of the tail is, as of yet, rather poorly defined in the literature, a wide range of possible motions will be explored in an effort to determine the most likely tail beat parameters.

While previous research has been conducted on force generation of ‘biologically inspired’ hydrofoils (Triantafyllou et al., 1993; Anderson et al., 1998; Lau and Kelso 2007), this set of experiments will address the topic with a level of bio-fidelity that is currently lacking in the literature. Specific hypothesis to be addressed are:

**1) Thrust generation will occur only under a specific range of tail motion regimes:**

While a wide range of mathematically possible motion regimes will be tested in the course of this study, it is believed that only a portion of them will be found to be

biologically relevant. This relevance will in large part be determined by their ability to produce a mean forward thrust over the course of a tail beat.

- 2) **Thrust generation will be close to, but slightly less than, the total drag expected on the fish:** While the caudal fin produces the majority of thrust in thunniform propulsion, it is commonly believed that the body of the organism primes the incoming water to allow for increased efficiency and/or thrust production. Possible mechanisms for this, such as constructive interference via vortex generation, redirection of water flow and boundary layer effects will not be examined in the course of this research, therefore overall thrust production is expected to be slightly less than seen in nature.
- 3) **Quasi-static modeling will under-predict thrust generated by the tail:** As will be discussed later, the quasi-static method of modeling thrust production does not take into account the inertial components of thrust generation (Webb, 1975; Blake 1983). It is therefore believed that this method will greatly underestimate total thrust production over the course of a tail beat.
- 4) **Key parameters used to define the tail motion (i.e. tail tip amplitude, frequency, etc) will, by themselves, not be able to predict thrust production in any meaningful manner:** Thrust production is a product of many interrelated parameters. While several of these parameters have been shown to have fairly constant relationships with factors such as swimming velocity, it is not believed that any single factor or combination thereof will be able to successfully predict thrust production.
- 5) **Secondary, ‘non-standard’ thrust generation mechanisms are possibly contributing to overall thrust production:** Previous studies examining pitching and oscillating foils in biological systems (Dickinson et al., 1999; Videler et al., 2004), have discovered

numerous mechanisms for generating lift and thrust not predicted by standard modeling (i.e. purposefully induced stall, wake capture, etc.). It is believed that in order to obtain such high levels of efficiency, thunniform swimmers may be taking advantage of similar mechanisms.

- 6) Calculated efficiency (disregarding torsional input) could be extremely high, possibly reaching above 90%:** While force generation or coefficient of thrust is an important measure of the effectiveness of a propeller, it is not the only one. The efficiency of the propeller is also of critical importance. Previous studies (Fish et al., 1996; Anderson et al., 1998) have shown that pitching and oscillating foils operating in the range of biologically inspired regimes can reach efficiencies of up to 90%. In order to calculate this efficiency 3 different measures are needed, the output (forward force), and the two inputs (lateral force and torsional force). As only one of the input forces are being measured (torsional forces will not be measured due to apparatus constraints), the calculated efficiency will be artificially high. Therefore, efficiencies of above 90% are possible.

## Background

### Biological

There are many ways to classify aquatic animals and their propulsive mechanisms. One standard method is to group animals based on broadly defined modes of body undulation. While recently some questions have been raised about the validity of this ‘classic’ method (Lauder and Tytell, 2006), it is still by far the most commonly accepted way of defining different swimming types. Using this method, aquatic animals are divided into five main groups along a continuum based on how much of their body is recruited in producing a propulsive wave (Figure 2). For example anguilliform swimmers (such as eels) generate a propulsive wave down almost the entire length of their body, while subcarangiforms (i.e. trout) generate a wave that is typically confined to the posterior half of the body. Carangiforms limit their body motions even more so, typically undulating only the rear third of their bodies. Thunniforms on the other hand take this confinement of motion to a much more drastic degree. For reasons that will be explained below, they typically confine their undulation to only the area including and posterior to the peduncle.

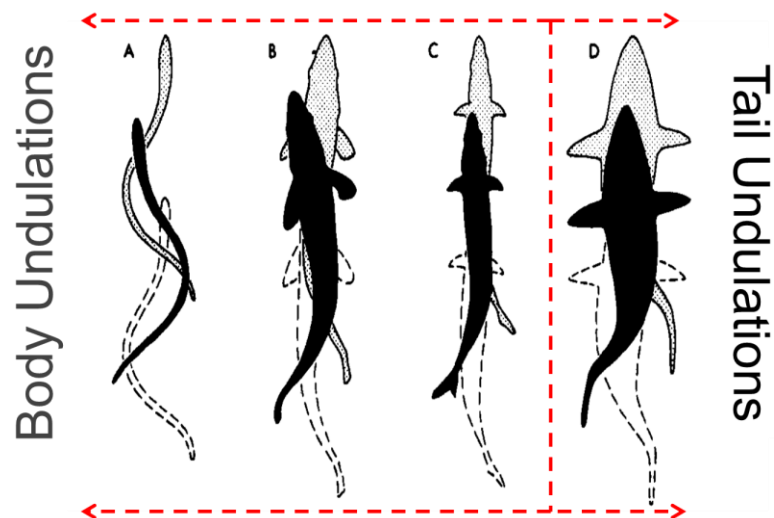


**Figure 2- Swimming Undulations:** Variation in swimming types ranging from (a) anguilliform, (b) subcarangiform, (c) carangiform, to (d) thunniform. While these are typically defined as a continuous spectrum, there is a distinct confinement of undulations to the tail of thunniforms (Figure modified from Lindsey, 1978).

For the most part, this localization of the undulatory wave to the posterior portion of the animal is accompanied by an increased cruising speed and higher efficiency (although it should be noted that this comes at the cost of reduced agility and acceleration, as per Sfakiotakis et al., 1999). These performance increases are made possible by the development of several morphological, physiological and kinematic adaptations common among Thunniform swimmers. For the purposes of this investigation, only the external morphological and kinematic features will be discussed.

The most noticeable and fundamental of these adaptations is a stiff lunate or crescent moon shaped caudal tail, with a cross section similar to that of a hydrofoil (Figure 3).

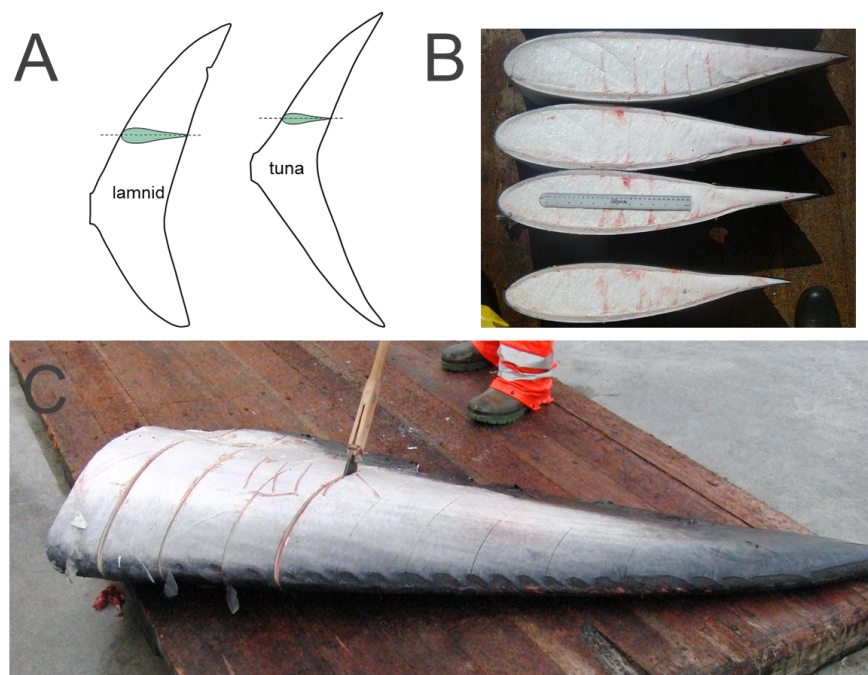


**Figure 3- Thunniform Hydrofoils:** Hydrofoil like cross sections as seen in caudal tails of tuna and lamnid sharks (a) (Figure modified from Shadwick, 2005) as well as fin whales (b, c).

By oscillating this tail back and forth (typically laterally), thunniform swimmers are able to generate thrust. However, while such lateral movements are required to propel the organism forward, it also produces drag on the rest of the body. This is for two major reasons. First, as the

body moves back and forth, it exposes a greater average surface area in the direction of fluid flow. This therefore has the effect of increasing overall drag on the body. Second, to move the body laterally, a great deal of water has to be accelerated and displaced (perpendicular to the direction of travel). As this requires a great deal of energy expenditure with virtually no return in regards to propulsion, it has the effect of greatly reducing overall efficiency. It is for these reasons that (as mentioned above) thunniform swimmers generally keep their bodies rigid, with only the far posterior end oscillating (Figure 4). Morphologically this is accomplished using several distinct features. For example, the peduncle is typically extremely tapered. As this is the portion of the organism that has to move laterally to allow for a complete range of tail motions, this ‘necking’ decreases both the area exposed to oncoming flow, and the volume of water that would have to be accelerated laterally for it to move freely. Furthermore the main part of the body (anterior to the peduncle) typically has considerable depth, thereby reducing the magnitude of any ‘recoil’ movement in this portion of the organism caused by the generation of tail undulations (Lighthill 1969).

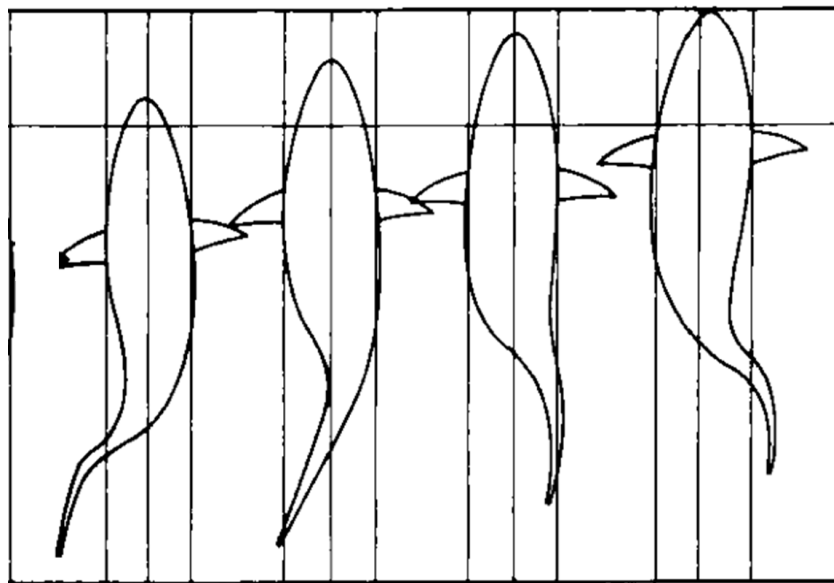


**Figure 4- Thunniform Undulations:** Confinement of propulsive oscillations to posterior end of the body in thunniform swimmers. (Figure modified from Magnuson, 1978).

These adaptations, along with a whole suite of others (both internal and external), can be found in a wide variety of high efficiency, large, open water aquatic animals. As these animals are in many cases only distantly related, and the associated characteristics are not typically basal, thunniform swimmers are a classic case study of convergent evolution.

## **Engineering**

As stated above, by passing their tail through water, thunniform swimmers are able to generate thrust. This is accomplished via a lift-based method as opposed to the drag-based method most commonly associated with other undulatory swimmers. Simply put, the drag-based method generates acceleration by producing an undulatory wave down the length of the organism. As this wave travels the body, each segment pushes water backwards along its length (as well as perpendicular or sideways), generating an overall reactive force in the direction of travel. By comparison, the lift-based method utilizes the pressure differential caused by flow past the caudal tail to generate thrust in a manner similar to that of an airplane wing generating lift. This method is believed to generate extremely high propulsive efficiencies (Triantafyllou and Triantafyllou 1995, as well as Anderson et al., 1998, both indicate the possibility of efficiencies in the range of 86-87%).

Most analytical approaches of analysis for thunniform propulsion can typically be divided into two main categories, being either resistive or reactive modeling. Resistive modeling for thunniform propulsion was first put forward by Parry in 1949 (Blake, 1983) and considers the tail to be a semi-static hydrofoil. This allows for the integration of the instantaneous thrust expected to be generated at any given point (via static testing), over an entire tail beat cycle in order to determine overall thrust. While this method has proved popular and is still commonly

referenced, resistive modeling does not take into account inertial forces (Webb, 1975; Blake, 1983), making it highly inaccurate (especially for large fast swimming fish).

Reactive modeling on the other hand, which was initially developed by Sir James Lighthill in 1969-70 (Blake, 1983), does take these inertial forces into account and is therefore considered far more realistic. A fluid mechanist by trade, Lighthill used 2D foil analysis common in engineering to help model thunniform propulsion. While a great deal of work has been done in updating and refining these mathematical models (Liu and Bose, 1993), a detailed background in advanced fluid dynamics is required in order to go into the matter in depth. Therefore, for the purpose of this study, the mathematical derivations and proofs associated with this line of reasoning will be omitted in favor of a more descriptive approach.

Essentially, reactive modeling is concerned with the momentum imparted on the water as a foil oscillates. This momentum takes the form of discrete sets of vortices in the wake of the foil. It is these vortices, their size, strength, orientation, relative positioning, etc., which determine the thrust produced. For example a thrust generating vortex formation will (when time averaged) actually produce a jet stream behind the object (Triantafillou et al., 2000), while an object producing drag (Reynolds numbers of approximately 40 to  $2 \times 10^5$ ) will generate a similar formation but with opposite vortex orientation (known as a Von Karman Street as seen in Figure 5).

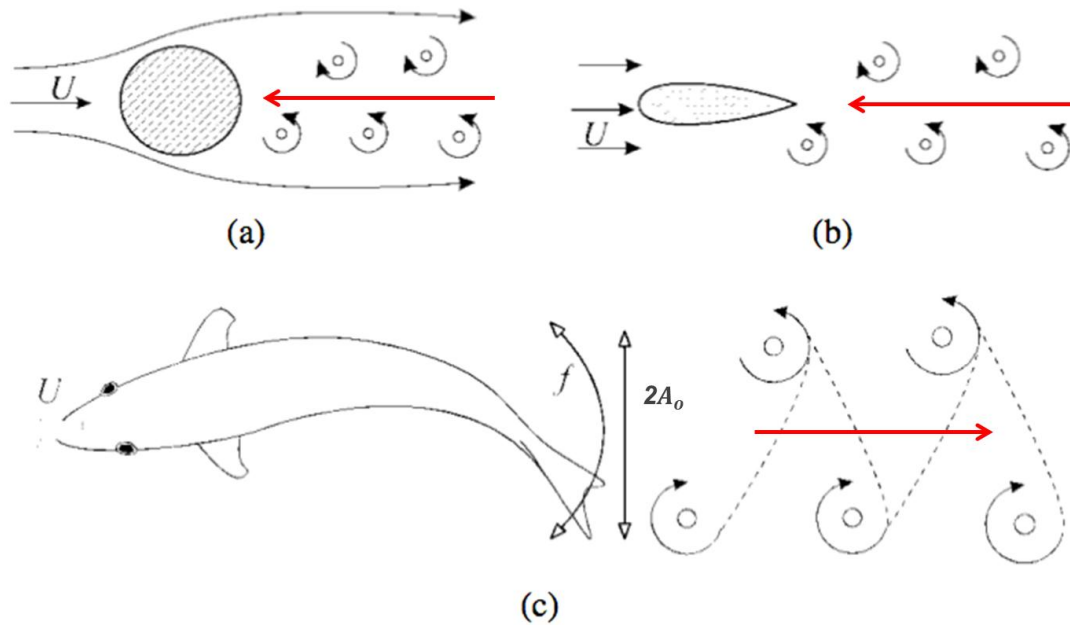


**Figure 5-Wake Visualization:** Drag producing Von Karman Streets behind bluff bodies (a, b), and thrust producing Reverse Von Karman Streets (c) (Figure modified from Sfakiotakis et al., 1999). Red arrows indicate direction of mean vortex induced water flow.

Therefore the parameters of motion for a given caudal fin that determine the formation of these vortices in fact determine the performance of the tail as a thrust producing foil. Triantafyllou et al. (2000), listed the following five ‘prime parameters’ as those which have the greatest effect on vortex formation in oscillating and pitching foils. Not surprisingly it is also these five parameters which allow (and in fact are required) for the complete definition of a foils motion:

- 1) **The relative position of the pitching axis:** This is the location about which the foil rotates its pitching angle, and is the standard reference point by which to determine the distance from centerline (i.e. yaw amplitude). In fish, this position can be located anatomically and for skipjack is assumed to be just anterior to the hypural plate (Figure 6) and can be seen in Figure 7.

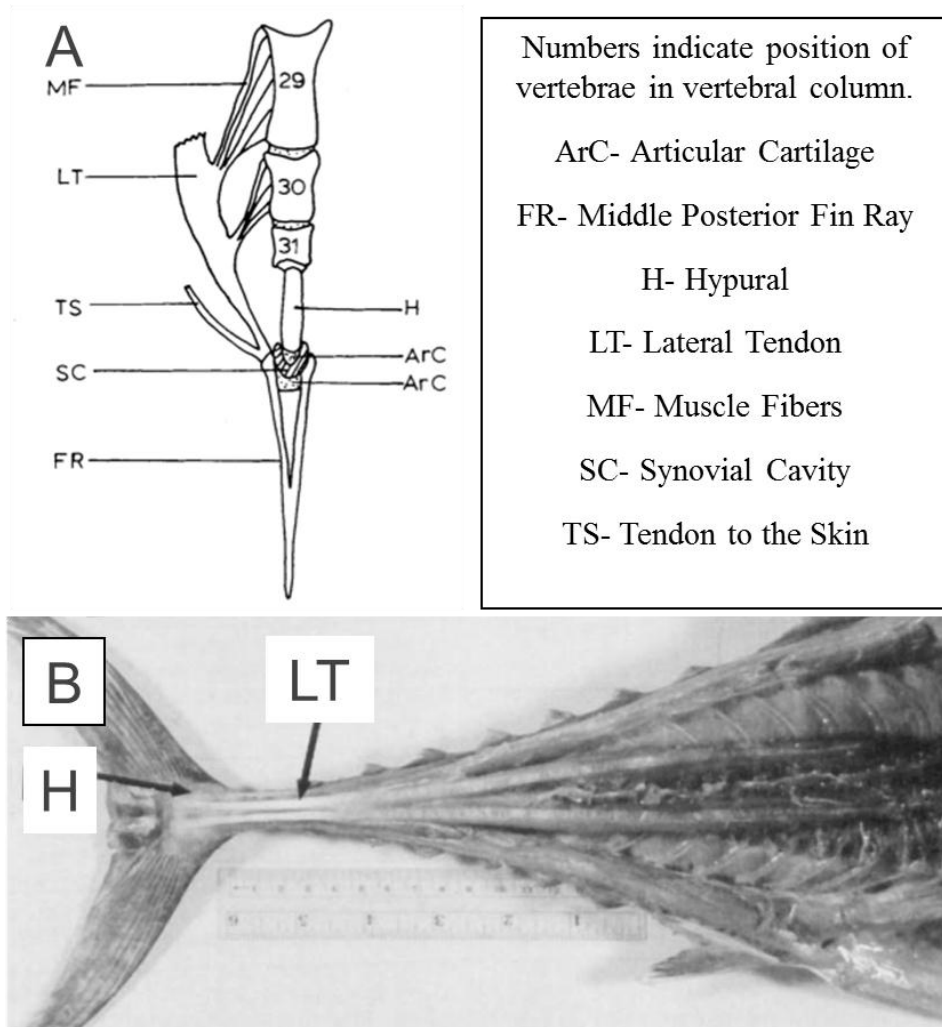


**Figure 6- Pitching Axis:** Schematic and picture of the caudal region of a *Scomber australasicus* (A) and a *Euthynnus alletteratus* (B) respectively. Pitching axis of the fin is assumed to be at the synovial cavity, just posterior to the hypural plate (Figure A modified from Fierstine and Walters, 1968, Figure B modified from Westneat et al., 1993).

- 2) **Amplitude of yaw motion normalized to the chord length ( $H_o$ ):** This is a dimensionless, relative measure of the maximum displacement ( $A_o$ ) between the foil pitching axis and centerline expressed as a ratio of the maximum yaw divided by the chord length:

$$H_o = \frac{A_o}{SMC} \quad \text{Eq. 1}$$

Where SMC is the standard mean chord length (Figure 7), and is calculated by dividing the planform area ( $\Lambda$ ) by the span ( $b$ ).  $A_o$  is the maximum amplitude of the yaw, describing the instantaneous displacement ( $A$ ) of the pitching axis as:

$$A = A_o(\sin(ft)) \quad \text{Eq. 2}$$

Where  $f$  is the tail beat frequency in rads/sec and  $t$  is the instantaneous time in seconds.

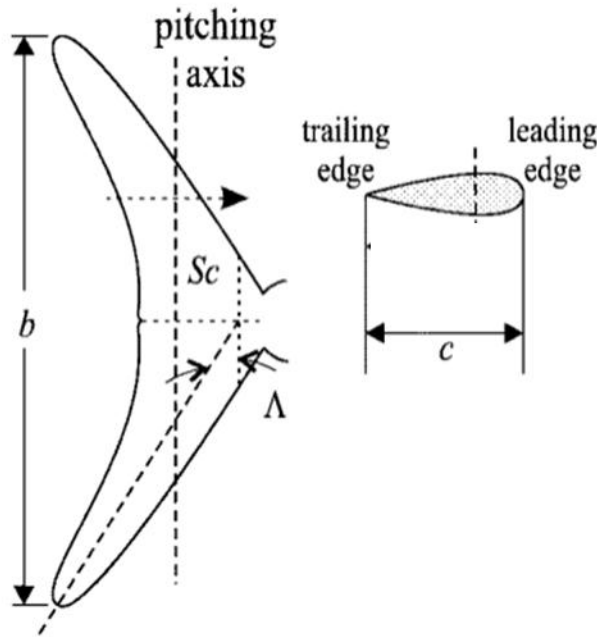


**Figure 7- Foil Characteristics:** Schematic of standard thunniform caudal fin showing the span ( $b$ ), pitching axis, sweep back angle ( $\Lambda$ ), chord length ( $c$ ) and planform area ( $Sc$ ) (Figure modified from Sfakiotakis et al., 1999).

- 3) **The Nominal Pitching Angle ( $\theta_o$ ):** The maximum angle of the foil relative to the free stream velocity of the fluid, where the instantaneous pitch angle ( $\theta$ ) is:

$$\theta = \theta_o \sin((ft) + \phi) \quad \text{Eq. 3}$$

Where  $\phi$  is the phase lag as described in point 5 (below). Care should be taken not to confuse the pitch angle ( $\theta$ ) with the angle of attack ( $\alpha$ ) which is the angle of the foil relative to the instantaneous local water velocity (Figure 8).

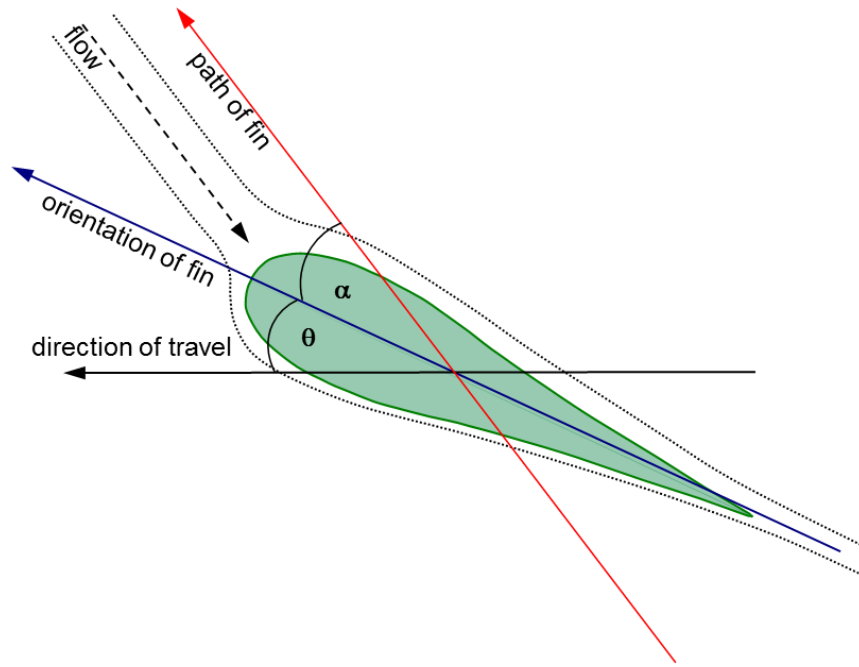


**Figure 8- Pitch and Attack Angle:** Diagram showing the pitch angle as well as the instantaneous angle of attack relative to the direction of travel, orientation of the fin and the path of the fin (Figure modified from Shadwick, 2005).

- 4) **The Strouhal number (St):** A dimensionless number used to compare the frequency of the foil relative to its maximum amplitude and free stream velocity. This is often used as a method of comparing the frequency of different oscillating foils by normalizing for the other two factors, and can be found as follows:

$$St = \frac{f(l)}{U} \approx \frac{f(2A_o)}{U} \quad \text{Eq. 4}$$

Where  $U$  is the free stream velocity of the water (in meters/second) and  $l$  is the characteristic length (in meters). It should be noted that, technically, the characteristic length is defined as the distance between two sequential vortices (Figure 5), however this

is usually approximated by either twice the pitching axis amplitude ( $2A_o$ ) or the tail tip amplitude depending on the source. While this distinction is minor, it is important and the particular Strouhal number being used at various points during this study will be stated explicitly.

- 5) **The phase lag ( $\phi$ ):** While both the pitching angle and the yaw amplitude of the tail are assumed to be identically sinusoidal functions, there is a time based phase lag as pitch always leads the yaw amplitude (Figure 9).

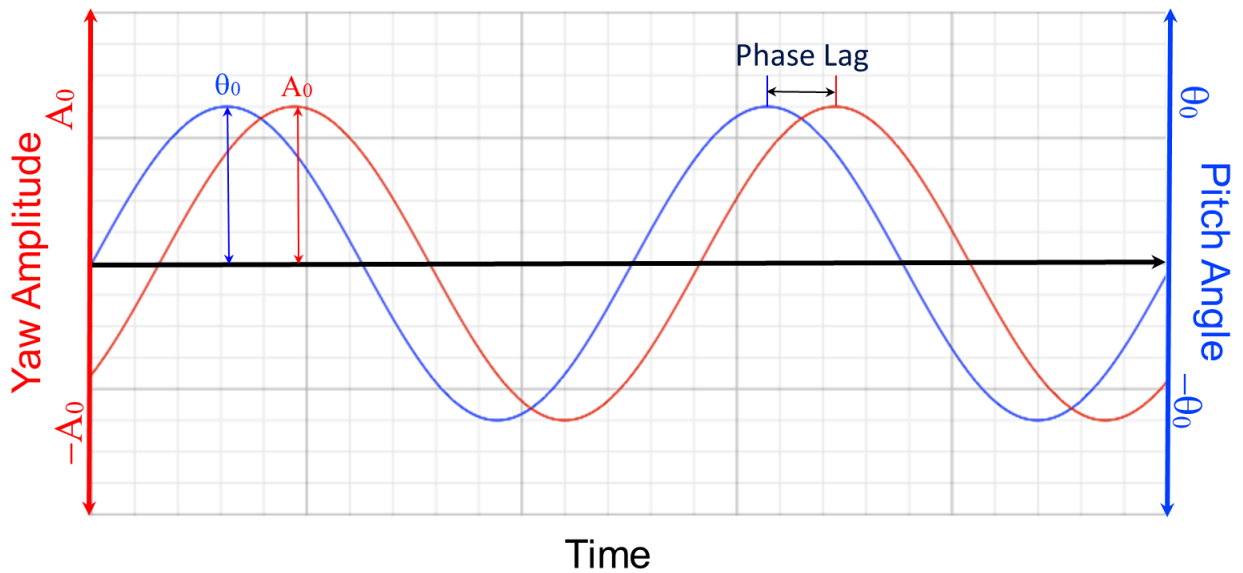


**Figure 9- Phase Lag:** Sample tail motion regime showing the yaw amplitude ( $A$ ), the pitch angle ( $\theta$ ), and the phase lag between the two ( $\phi$ ).

## **Methods**

The following section describes the methodology employed throughout the course of this project, and has been divided into the following subsections for ease of reading. While these subsections are not intended to be taken as a chronological list of events, they do provide a step-by-step outline of the research conducted:

- 1) Creating Tail Models
- 2) Specimen Selection
- 3) Water Tunnel Selection and Calibration
- 4) Defining Motion Parameters
- 5) Apparatus Construction
- 6) Data Collection

### **Creating Tail Models**

The first step in designing and constructing a test apparatus was to determine the methods available for creating models of the tail specimens. This is in large part due to the possibility of dynamically scaling the models (i.e. changing the size of the model). Essentially dynamic scaling involves maintaining constant flow conditions in spite of changing flow parameters (i.e. free stream velocity, viscosity, foil size, etc), by modifying other flow parameters. This is based on keeping a constant Reynolds Number as shown below:

$$Re = \frac{lU}{\nu} \qquad \text{Eq. 5}$$

Where  $l$  is the characteristic length of the object (typically the standard mean chord length), while  $U$  and  $\nu$  are the free stream velocity and kinematic viscosity (the dynamic viscosity divided by the density) of the fluid, respectively.

So for example, if one wanted to run tests on a hydrofoil traveling through water at 1m/s, but only had a flow tank that would allow 0.5m/s, identical flow conditions could be generated by doubling the characteristic length of the foil. Similarly if a wind tunnel were to be used instead of a water tunnel, then the velocity would need to be increased to approximately 13 m/s (as water has a kinematic viscosity 13 times greater than air). For these reasons, having a dynamically scalable model, would allow for testing in numerous test facilities and under conditions that would otherwise not be useful.

Therefore the first and preferred method of modeling the specimens involved generating a computer model of the tail and then using that to fabricate a physical model. As the shape of the specimen would have been completely digitized, any alterations to it (i.e. scaling) could be made with relative ease. In order to do this, the preserved specimens were taken to the Imager Lab at the UBC Department of Computer Sciences, where their shape was digitized using a 3D laser scanner (Cyberware Scanner). This data would then have been imported into a computer assisted drafting (CAD) program, such as ComSol Multiphysics or Solid Works. At this point the model could be scaled or modified as required, before being physically created out of a stiff, insoluble, plastic resin using a Rapid Prototyping Machine.

Unfortunately, the digitizing process did not prove accurate enough for use with the given specimens. This was due to the process in which the 3D model was constructed using the Cyberware Scanner. Essentially, the scanner takes images of the target from eight different angles and then combines them to form a digitized model. However, as the trailing edge of the

specimens become paper thin (0.01mm), the imaging software could not resolve what surface belonged on which side of the tail. This consistently resulted in a computer model of the tail in which the two external surfaces actually intersected generating an object that would be physically impossible to create (Figure 10).

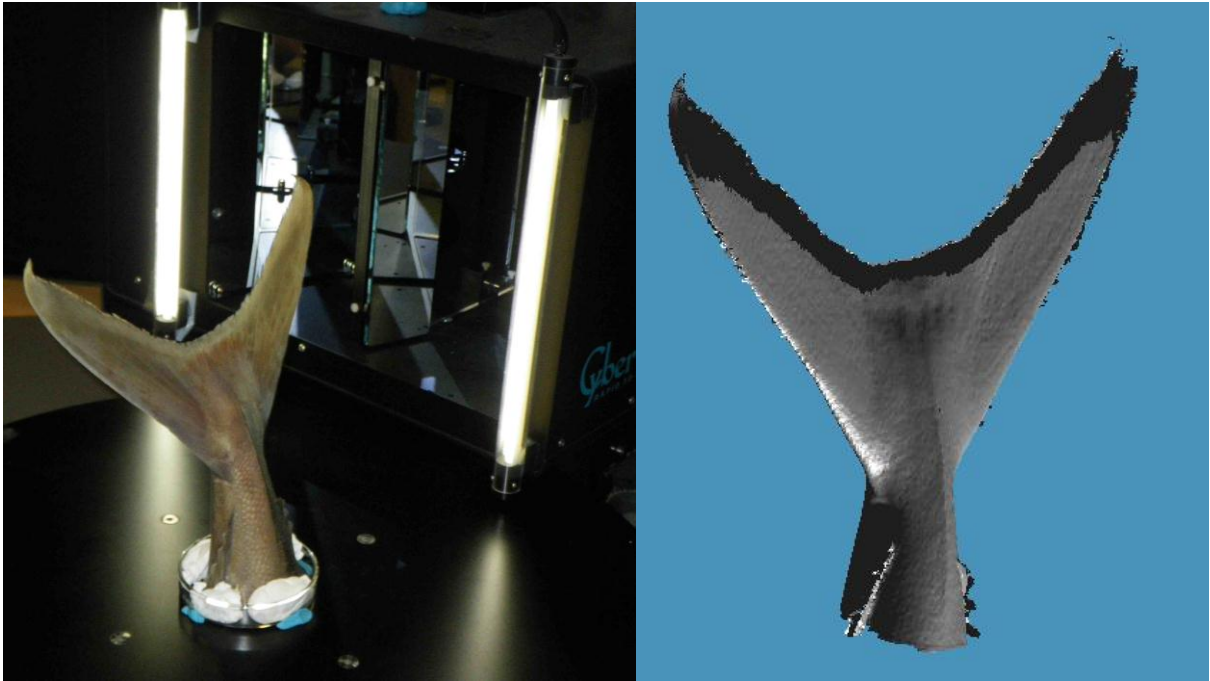


**Figure 10- Laser Scanner:** Scanning apparatus with Yellowtail Jack tail (a) and the computer generated model of the Yellowtail Jack tail (b). Dark fringes in the model indicate areas of surface intersection.

While there are other methods to generate a digitized model of the specimens (i.e. CT or MRI scanners), they were determined to be inappropriate for the current study. Instead, the option of dynamically scaling the specimen was abandoned in exchange for a simpler and more accurate modeling method. This was done by creating a direct mould and cast of the specimens using Tropicalgin (an alginate impression material) as the mold and Flexacryl Hard (an acrylic resin) as the casting compound (detailed instructions on how this was done are given in Appendix A). While this only allowed for a 1:1 scale model of the tail to be created, the speed and accuracy with which these models could be made were determined to be very favorable (Figure 11).

Furthermore, it quickly became apparent via observation that the material properties of the Flexacryl cast were surprisingly similar to that of the actual specimens.



**Figure 11- Tail Model:** Final model tail made of Flexacryl superimposed on top of the original tail specimen. Parallel lines indicate location of material testing constraints, while the circled cross indicates location of test.

While material properties such as stiffness and hysteresis are often overlooked in similar studies (Anderson et al., 1998; Lau et al., 2004; Chong et al., 2009), recent work has shown that they can have a major impact on thrust generation (Blickham and Cheng, 1994; Lauder and Madden 2006; Lauder et al., 2007). However, as the specimens are not made of a homogeneous material, it is quite difficult to accurately quantify their material properties. Therefore in order to compare the specimens and the models, a more qualitative approach was taken. Both a specimen and its identical model were loaded onto an MTS 858 Mini Bionix test system and cycled from a neutral position to a maximum deflection of 3cm at a rate of 2.5 Hz (approximately the frequency of a small skipjack at a routine cruising speed). Both tests were run using identical restraining methods and loading points at approximately half way down the chord length and one quarter the span of the tail (Figure 12). The resultant force measurements were recorded and a Matlab code

was created in order to filter and analyze the data. Data was taken at approximately 100 Hz, and as there was a large amount of noise in the signal (likely due to the mechanical instabilities inherent in bending a cantilever beam) a 10<sup>th</sup> order Butterworth low pass filter set at 10 Hz (or approximately 0.2 of the nyquist frequency) was used. The nyquist frequency is considered the highest filter frequency allowable for a sample and is usually taken as half the sampling rate (in this case 50 Hz). Using this method both the stiffness and hysteresis of the model and specimen (specific to the point tested) were determined (see Figure 13). Also, it should be noted that all matlab filtering was done using a zero phase shift digital filter. While both material properties were shown to be significantly different between the model and specimen ( $p=0.05$ ), it should be pointed out that this is a statistical distinction and such a small difference is likely not biologically relevant.

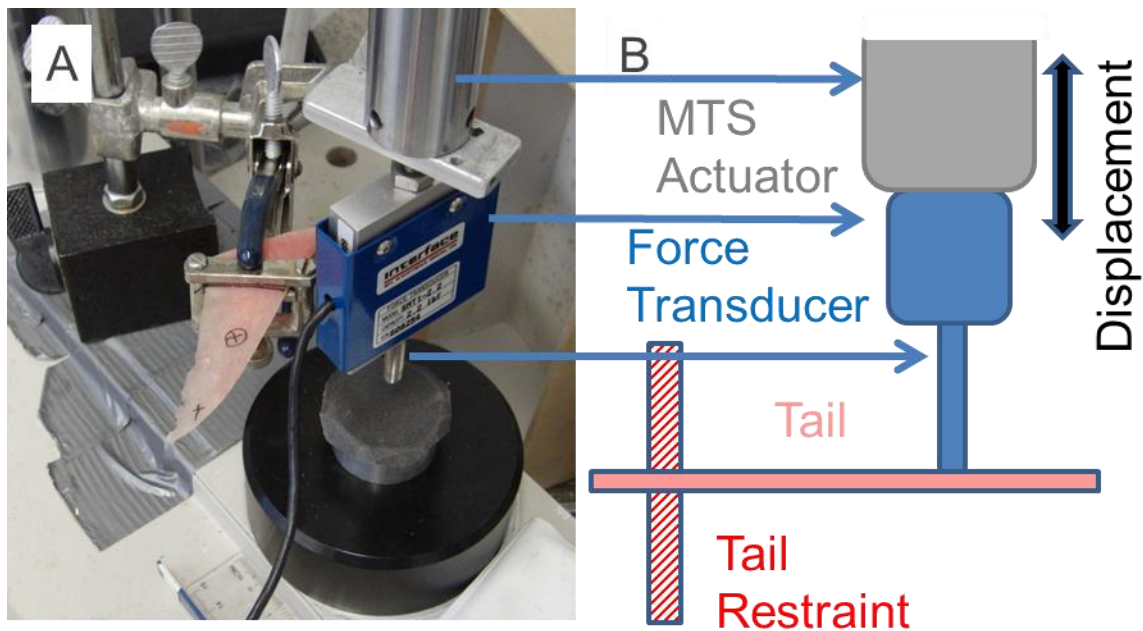


**Figure 12- MTS Setup:** Picture of MTS system with model tail (A), and a schematic showing system operation (B). Circled cross indicates location of testing point.

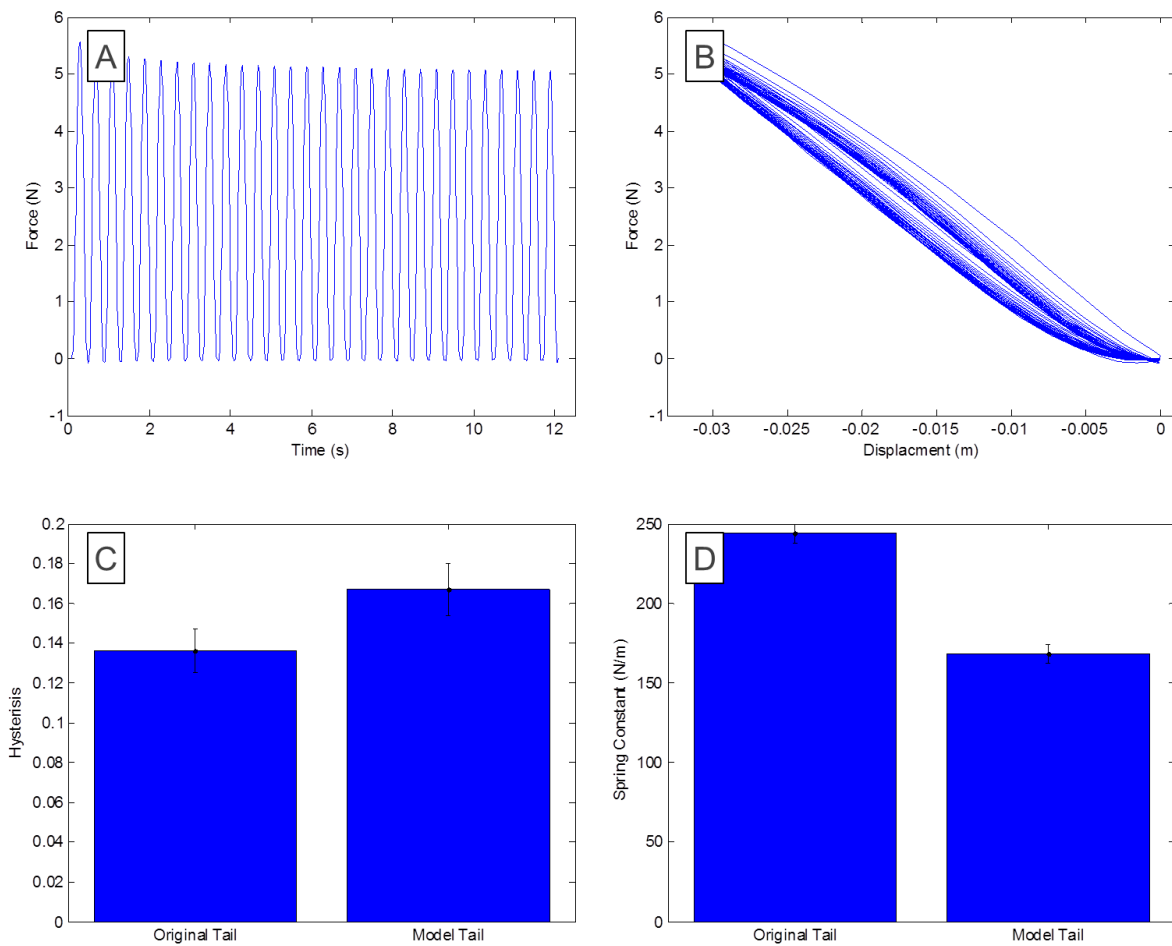


**Figure 13-Material Property Comparison:** Filtered Force-Time (a) and Force-Displacement (b) data from cyclical loading of tail model. Data from six trials is summarized showing significant statistical difference between hysteresis (c) and stiffness (d) of the original tail and its model.

This of course makes two major assumptions about the caudal fin structure and function. Firstly, it assumes that the process of preserving the specimens (as described in the following section, Specimen Selection), did not significantly alter the material properties of the fin. This is likely the case as a large portion of the tail structure is made of boney fin rays, which would be largely unaffected by the chemical treatment used. There is also however considerable soft tissue (muscle, tendon, ligaments, etc.), located in the tail whose material properties may be effected to some degree. As these tissues likely only serve a secondary role as far as tail structure is concerned, it was assumed that any changes to their material properties would be negligible for the purpose of this study. The second assumption being made is that the caudal fin itself is

essentially a passive member. That is to say that while external forces may act on it (i.e., the fish body, surrounding water, etc.); it does not generate any internal forces through such methods as muscle contraction. Therefore any deformation and changes in shape occurring to the tail would be entirely the result of these external forces. While there is evidence in other fish, such as mackerels, to show that this is not the case (Gibb et al., 1999), and the positioning of certain muscle groups indicates they may be used to modify the fin shape while swimming (Westneat and Wainwright, 2001), this has yet to be proven for tuna. Furthermore some of these muscle fibers are greatly reduced in tunas compared to similar fish, resulting in essentially ligament like structures (Westneat and Wainwright, 2001). Therefore for the purposes of this study, while internal muscles likely have some impact on tail shape during swimming, it is assumed that this effect is minimal. That being said, both these assumptions should be examined in further detail and validated, as described in the section titled Future Directions.

It was therefore decided that models of the chosen specimen would be made using this mold and cast method. With the knowledge that the dynamic scaling factor would be locked into a 1:1 ratio, it was now possible to determine both the most appropriate specimens to be used as well as identify various water flume candidates.

### **Specimen Selection**

Several different types of thunniform swimmers were considered when trying to determine a model species for this study. The initial options were quite broad, covering a range of teleosts, lamnids, and cetaceans. In the end, largely due to logistical reasons and available in vitro data, it was determined that skipjack tuna (*Katsuwonus pelamis*) would be best suited for the purpose of this research.

The primary reason for this choice is that skipjack are one of the smallest thunniform swimmers. Not only did this make models of their tails easier to create and handle, but it also played a key role in limiting the necessary size and speed of the water tunnel used in the course of these experiments. Furthermore, there is a great deal of published work on the kinematics of skipjack swimming currently available (Yuen, 1966; Fierstine and Walters, 1968; Magnuson, 1978; Knower et al., 1999; Brill and Bushnell, 2001). These data (which included ranges for tail beat frequency, swimming velocities, Strouhal Numbers, and tail tip amplitude) proved to be incredibly important in defining realistic motion parameters for the test apparatus.

For these reasons, three samples of skipjack tails were acquired from the Phleger Institute of Environmental Research, Oceanside, California, USA. Each sample consisted of approximately the posterior quarter of the entire animal (full body lengths were: 64, 61 and 57 cm). The samples were treated in formaldehyde and then placed in an ethanol water mixture, taking care to ensure the tips of the tail were not deformed during storage. At this point the 57 cm full-length specimen was determined to be in the best condition (less wear along the edges, limited to no curling of the tips, etc) out of the three tails and was used as the primary test specimen for the remainder of the project.

## **Water Tunnel Selection and Calibration**

### **Selection**

There were several major constraints that needed consideration in determining an appropriate water tunnel for the course of this study:

- 1) The cross-sectional size of the tunnel had to be large enough to accommodate the full range of motion expected by the tail model, plus leave additional leeway to minimize any apparent wall effect.

- 2) Sustainable and laminar water speeds of approximately 1 m/s needed to be attainable.
- 3) The test section of the tunnel needed to be accessible from above, with room for the test apparatus.
- 4) Associated Particle Image Velocimetry equipment would have been useful in conducting additional tests. (Optional)

In order to meet these requirements several tunnels and flumes at UBC (Biological Sciences, Mechanical Engineering) and associated facilities (Vancouver Aquarium, Bamfield Marine Science Center) were examined. In the end, largely due to the cross-sectional and velocity constraints, only one water tunnel was deemed usable. This was the Loligo Model 90 swim tunnel located at the UBC Department of Zoology, which provided a working cross section of 240 by 250 mm and reached speeds of up to 1.3 m/s.

Unfortunately, there were some drawbacks to this particular flow tank. Firstly and most importantly, due to the small size of the tank a variable flow profile and turbulence could not be completely eliminated despite the use of flow straighteners (a flow screen was not deemed feasible given the size of the tank). While these factors could not be eliminated, attempts were made to mitigate their effect as described below. Other minor yet notable drawbacks to this flow tank included the fact that at maximum oscillation and pitch amplitude the tip of the tail would reach within 5.2 cm of the wall. It is believed however that any wall effect caused by this would be minimal as it would only occur infrequently, and even at these times, the bulk of the tail would be considerably further away from the tunnel walls than the tip. Finally, it was unfortunate that this particular tank did not have any associated PIV equipment, as this would have allowed further data collection via flow visualization.

## Calibration

In order to calibrate the water flume, a cross section of the testing area was divided into 16 points. The velocity at each of these points was then recorded at 6 equally spaced settings over the applicable motor operating range (see Figure 14). The flow velocity at each location/setting was measured using a Hontzsch HFA U363 flow probe. An analog output fed the data directly to a computer (via a BioPac MP100 data collection system) where it was digitally filtered and recorded in real time using AcqKnowledge 3.8.2.

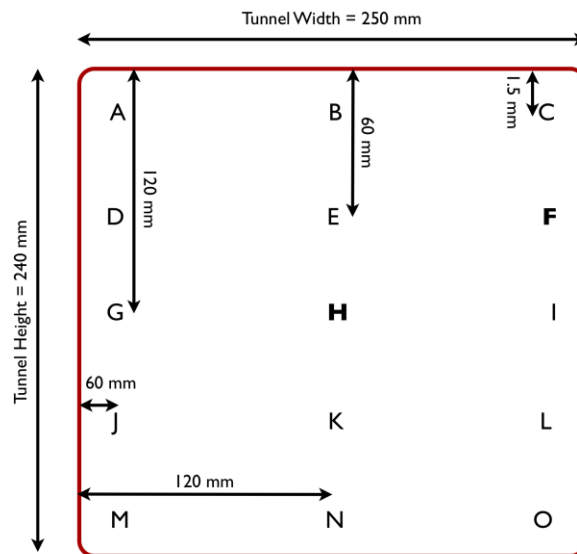


**Figure 14- Test Section Diagram:** Diagram showing the location of velocity measurements in the test cross section of the flow tank. Highlighted locations (F and H) indicate location of repeatability tests. Tests were conducted at motor settings of 12, 14, 16, 18, 20 and 22 Hz.

One important point to note is that the flow meter had a maximum sampling rate of 1 Hz (likely due to the rotary nature of the probe). This would typically produce a stepwise function (assuming a collection frequency greater than 1 Hz), however it was quickly noticed that there was considerable noise in the signal (possibly from nearby EM sources). In order to produce an accurate reading from this data set, the following steps were taken:

- 1) The signal was oversampled at a rate of approximately 200 Hz for 32 seconds (the first and last second of every sample was discarded).

- 2) The oversampled data was then filtered by the data collection software using a low pass filter set at 5 Hz (0.05 of the nyquist frequency) with a Q factor of 0.707 (equivalent to a Butterworth filter) .
- 3) The data was then sub sampled at 12.5 Hz and smoothed using a three point average to reduce both the data set size and return it to its true stepwise nature. An average was taken to determine the ‘true reading’ for each one second interval.
- 4) The mean velocity was then calculated over the entire 30 second sampling period.

Repeatability of this method was verified by testing two randomly chosen locations (F and H in Figure 14), five times at three different motor settings (10, 20 and 28 Hz). The flow meter setup was disassembled and the motor settings were completely reset between each run to avoid any bias. Using this method it was determined that the standard deviation between runs (at the same location and motor setting) was within the same order of magnitude as the standard deviation within a run (9.2 mm/s between runs at the same setting vs. 15.0 mm/s within an individual run). Furthermore, none of these values ever exceeded 3% of the true free stream velocity. This indicated that the amount of error due to setup and repeatability issues during calibration was minimal.

The data collected were used to interpolate a series of velocity profiles covering the entire range of motor settings (Figure 15). Using this data it became clear that the test section had a very skewed flow profile, with the highest velocities located at the outside lower corner of the section. While normally this would pose a major concern for testing within a flow tank, in this case the tail model would only travel through a small portion of the test section (along the top of the tank). This smaller subsection was determined to have a much more homogeneous flow profile

(as indicated by the minimal standard deviation shown in Figure 16), and was therefore deemed usable.

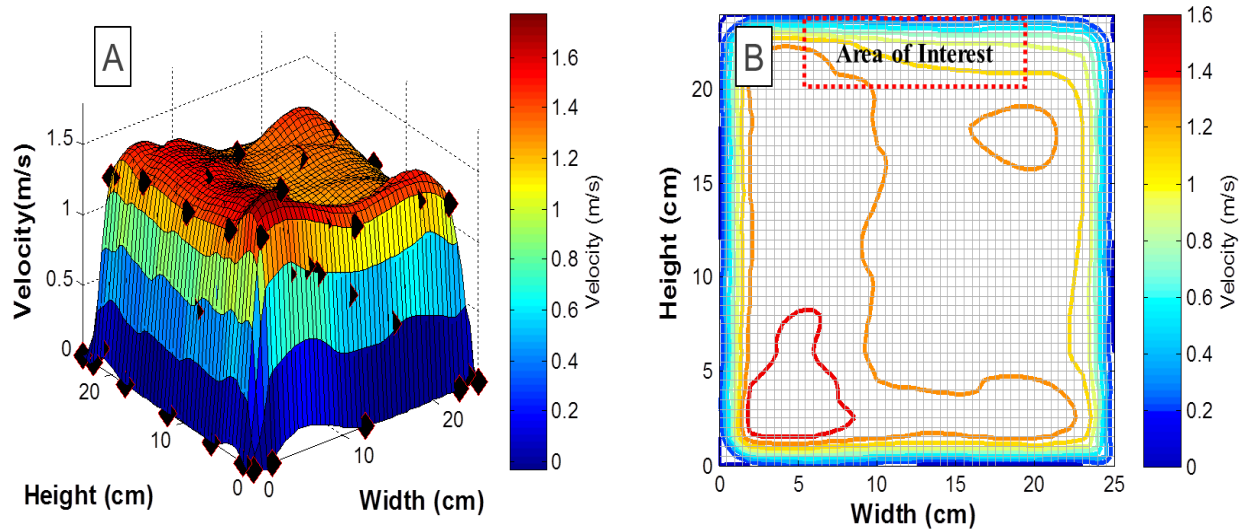


**Figure 15- Test Section Velocity Profile:** Sample velocity profile of water flume test section at a motor setting of 22 Hz (A) and a topographic image of the same velocity profile (B). Diamonds indicate velocity test locations or points of zero velocity according to no-slip wall conditions. Section of the cross section in which the tail model will be present is marked off as the areas of interest.

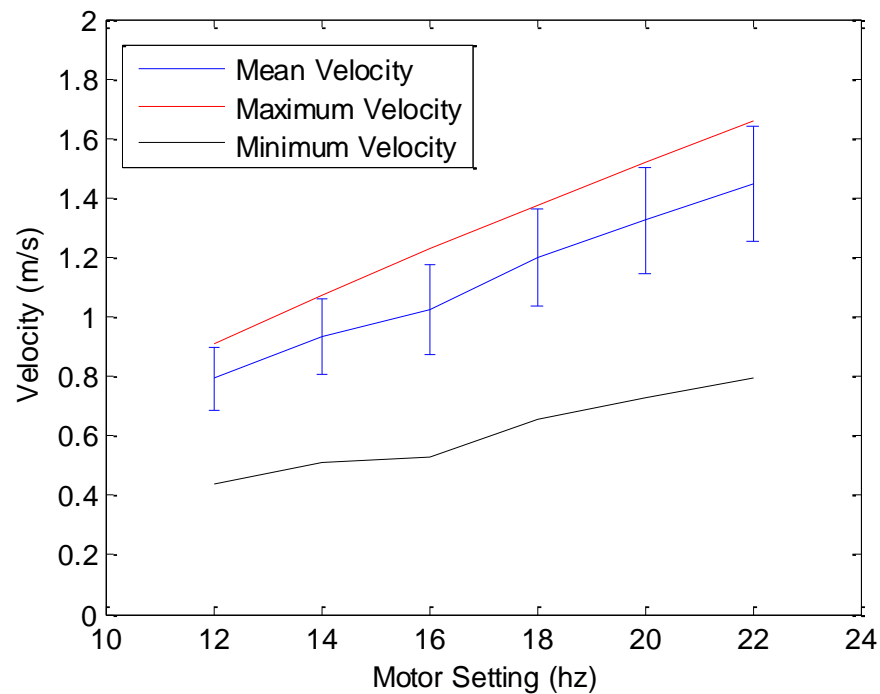


**Figure 16- Test Section Calibration:** Average velocities (standard deviation bars shown) of flow in region of interest of the water tunnel versus motor setting. Red line indicates maximum velocity recording, black line indicates minimum velocity recording and the blue line indicates mean velocity recording.

## Boundary Layer

Finally one item that should be clarified is the over exaggerated boundary layer seen in the flow profile along the walls of the tank (Figures 15 and 16). This is largely an artifact due to the fact that a rotary vane (diameter equal to 25mm) was used as the flow meter, meaning the slower velocity along the wall was disproportionately weighted on the rest of the 25 mm closest to the wall.

In order to confirm this, an analytical approach was used to determine a more realistic value for the boundary layer thickness (the point away from the wall at which the local water velocity reaches approximately 99% of the free stream velocity). This was done assuming both laminar and turbulent flow conditions for which the boundary layer thickness would be approximately either 0.34 cm or 1 cm respectively (calculations are shown in Appendix B). While the Reynolds number associated with this calculation is considerably lower than what would typically be associated with turbulent flow ( $3.6 \times 10^5$  vs.  $10^6$ ), upstream conditions (i.e. motor) are believed to contribute to the early onset of turbulence. Therefore it was assumed that the flow is likely at some intermediate stage, and that the boundary layer is somewhere between the 0.34 cm and 1cm values, confirming it is much smaller than the tested flow profiles indicate.

## **Defining Motion Regimes**

As noted above, there are five key parameters that are required to completely define the motion of a foil. While there is a great deal of kinematic data available for swimming skipjack, the majority of these five parameters are neither clearly defined nor measured in the common literature. In fact, the most common measures available in the literature defining tail motion were typically frequency, tail tip amplitude and tail tip Strouhal number. With the exception of the tail beat frequency these measures are in fact non-unique results of the five defining

parameters. That is to say that for a given tail tip amplitude, there could be a number of different defining parameter combinations that would cause it. Therefore it was decided that wide ranges for these five parameters would be examined and their resultant tail tip amplitude and tail tip Strouhal number would be compared to literature values to determine feasible test parameters. In order to accomplish this, the following methodology was used:

- 1) A test velocity of 1 m/s was chosen for the water flume. This would be equivalent to 1.75 body lengths per second (Bl/s) for the chosen specimen of 570 mm. This velocity falls well within the ranges of expected continual swimming for skipjack as discussed by Brill and Bushnell, 2001 (1.6-2.2 Bl/s) and Klower et al., 1999 (1.5-3.7 Bl/s).
- 2) Tail beat frequency was calculated as a function of velocity as per Klower et al., 1999:

$$f = 0.96\left(\frac{Bl}{s}\right) + 1.43 \quad \text{Eq. 6}$$

This results in an expected mean frequency of approximately 3Hz. The range to be analyzed was determined to be +/- 20% of the mean.

- 3) As an accurate range of the phase lag was not known (apart from the fact that the pitch leads the yaw), a wide range of 0-80 degrees was chosen. Using a standard hydrofoil setup, Anderson et al. (1998), estimated that peak efficiency would occur at approximately 75 degrees, however that experimental setup was significantly different than the current study.
- 4) The nominal pitch angle was, again, not well defined in the literature. However a range of 0-90° was deemed to be most realistic. 0° indicates that the tail would always remain parallel to the free flow conditions at all times, while 90° indicates that the tail, at some

point would be completely perpendicular to the free flow. As both of these extremes are not realistic for both biological as well as fluid dynamic reasons, the true range must lie somewhere in between them (Fierstine and Walters, 1968, indicated that skipjack could reach angles of attack of up to  $100^\circ$  however this appeared to be rare).

- 5) The amplitude of the pitch axis was determined essentially post-hoc. It was known that this amplitude would never exceed the maximum tail tip amplitude (based on the phase lag and pitching angle ranges), so while a wide range was used initially, it was eventually lowered down to 15-60mm.

With these motion parameter ranges in mind, discrete values were chosen for testing as displayed in Table 1. A matlab program was then created to go through all possible permutations of these parameters and calculate the resultant tail tip maximum amplitude and tail tip Strouhal number. If these two resultant parameters were found to be within the range seen in literature, then the defining parameters were considered to be feasible and were recorded for testing. In general the tail tip amplitude had to be between approximately 8-15% of full body length as per Fierstine and Walters (1968) and Strouhal number had to be between 0.25-0.35 as per Triantafyllou et al. (1993). Using this method, the number of possible parameter combinations (or motion regimes) to be tested was dropped from 300 to just 43 (for a full listing of all 43 test parameters used refer to Appendix C).

Parameter	Possible Test Values
Frequency, $f$ (Hz)	2.4, 2.7, 3.0
Phase Lag, $\phi$ ( $^{\circ}$ )	0, 20, 40, 60, 80
Nominal Pitching Angle, $\theta$ ( $^{\circ}$ )	20, 35, 50, 65, 80
Maximum Yaw Amplitude, $A_o$ (mm)	15, 30, 45, 60

**Table 1- Test Parameter Values:** Possible test parameters whose combinations were examined for resultant tail tip amplitude and Strouhal number.

## **Apparatus Construction**

### Design Selection

With the motion parameters defined, the specimen models created and the water flume chosen, it was now possible to design an apparatus to conduct the testing. Ideally the apparatus would sit above the water flume and hang the tail into the water (through a mirror plane) via a shaft that could both rotate and move laterally across the working section. It was quickly determined that there were two main possible methods by which this could be accomplished.

The first method considered was having a fully programmable linear actuator moving a platform back and forth over the tank. This platform would support another fully programmable rotary actuator that would change the pitching angle of the tail model. This method had the benefit of making both the amplitude and the pitching motions completely programmable allowing for any motion pattern or combination of patterns to be used. Additionally the relationship between the pitch and the amplitude could be changed at will and overall would have provided an incredible amount of flexibility in running experiments. Unfortunately, due to the rapid acceleration and deceleration associated with the proposed motion regimes and the weight of both the platform and rotary actuator, the force demands on the linear actuator would have been incredibly high. In order to address this issue a brushless motor positioning stage would have been required,

raising the cost of such an apparatus significantly. Preliminary cost estimates of developing this apparatus design were in the range of \$20, 000; therefore an alternative design was pursued.

The second possibility was to drive the apparatus with a single DC motor and use a series of scotch yokes to create both the amplitude and pitching motions. While this greatly reduced the flexibility of the testing (new parameters could not be built into the apparatus after construction), and provided several technical difficulties (transferring rotary motion from a stationary DC motor to a moving cart), it was determined that this was the most feasible course of action.

To this end, the Department of Zoology machine shop constructed a custom made apparatus fondly referred to as “Da Bruce” which is described in the following section.

### Design

Figure 17 shows the final test apparatus and its key features. Below these key features and their purposes are described in detail.

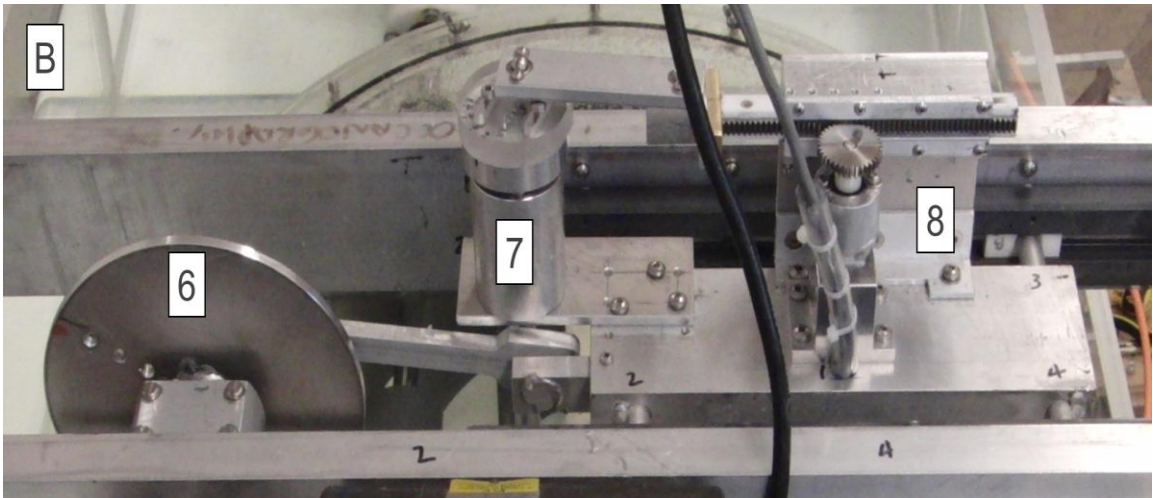
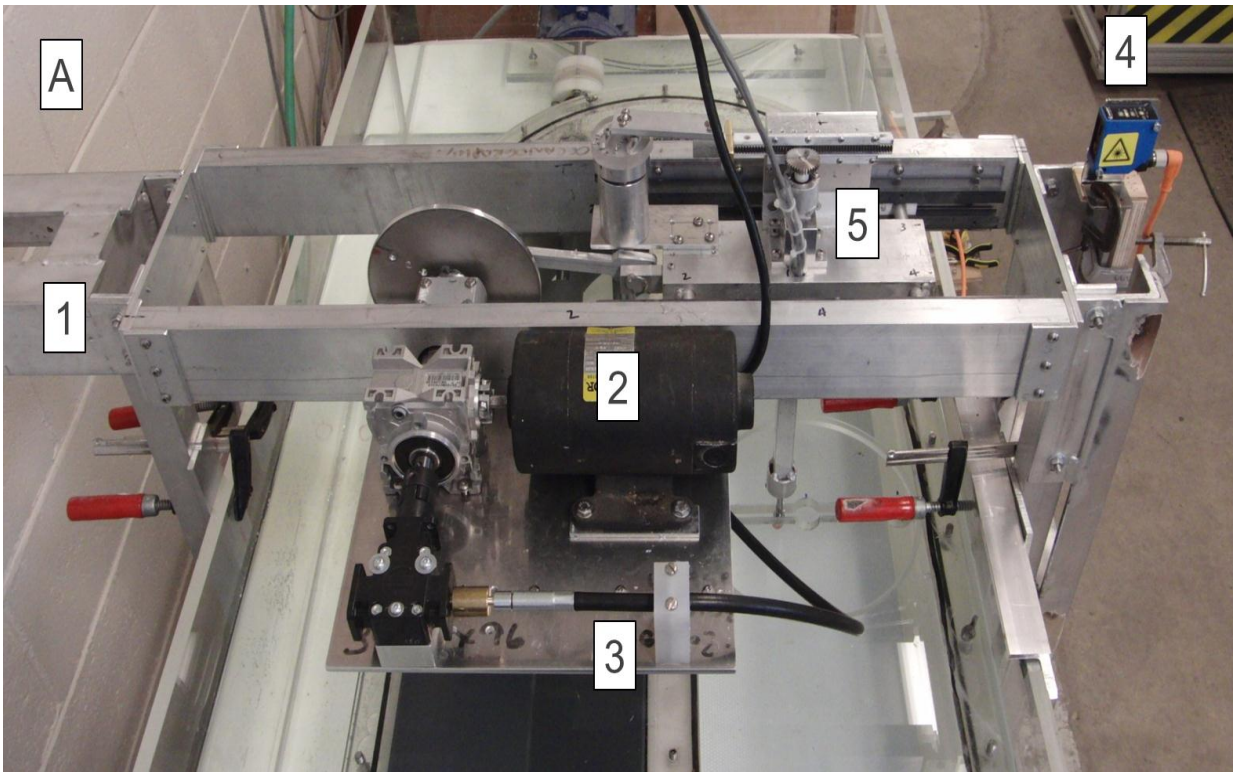


**Figure 17A- 'Da Bruce':** Various views of the custom built test apparatus: A) Overall view, B) Close up view, C) Underside view. Description of all the different components and their function are located in the text.

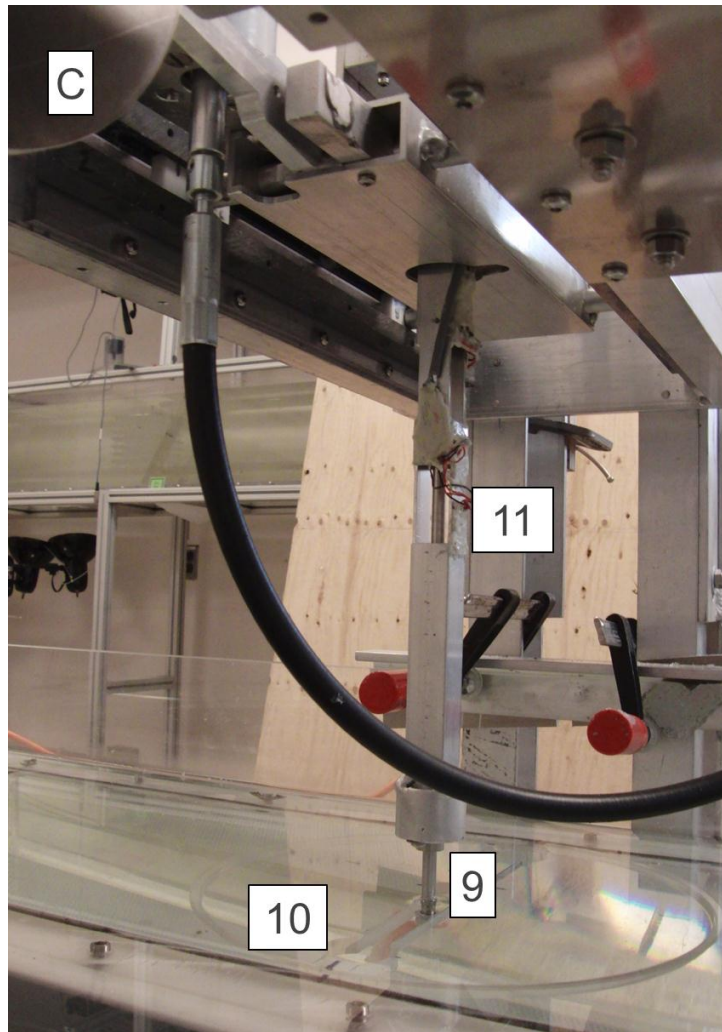


**Figure 17B- 'Da Bruce':** Various views of the custom built test apparatus: A) Overall view, B) Close up view, C) Underside view. Description of all the different components and their function are located in the text.

- 1) **Aluminum Frame:** The apparatus is suspended over the flow tank using a stainless steel frame. This frame was bolted to both the nearby wall and the floor in order to reduce vibration and ensure proper and stationary positing relative to the tank.
- 2) **DC Motor with a Differential Reducer:** A single DC motor is used to run the apparatus, therefore a differential needs to be used in order for it to rotate both the amplitude and the pitch cams. This differential has two output shafts at 180 degrees to each other, and also functions as a 7:1 reducer off the motor.

- 3) **Flexible Drive Shaft:** In order to power the pitch cam, rotary motion needed to be transferred from the stationary motor plate to the moving cart. This was accomplished by using a flexible shaft that was held stationary at one end, but moved with the cart at the other. While this ensured that both the amplitude and the pitch shared the same frequency, the phase lag could be adjusted by simply decoupling the flexible shaft, rotating the pitch to the desired phase lag, and then reattaching.
- 4) **Laser Sensor:** In order to record the exact position of the cart at any given point in time, a laser displacement sensor used (Wenglor CP35MHT80). It was attached to the frame, perpendicular to the cart motion, and pointed at a stationary location on the cart. This provided an analog signal directly to the data collection hardware.
- 5) **Cart:** The cart is the platform which holds the rotary cam, rack and pinion, as well as the box beam/shaft supporting the tail. It moves back and forth along a plastic track using four nylon gliders. Powered by the amplitude cam, its motion is equivalent to the amplitude motion of the tail itself.
- 6) **Amplitude Cam:** This spinning disk had a direct link to the cart, and determined its amplitude of motion. By changing the location of the linkage point relative to the center of the disk, the amplitude of the cart could be adjusted.
- 7) **Pitch Cam:** This cam drives the rack controlling the pitch of the fin. Powered by the flexible shaft, the maximum pitch angle is controlled by adjusting the attachment point of the linkage to the rack relative to the cam's center.
- 8) **Rack and Pinion:** The rack and pinion is the mechanism by which the linear displacement generated by the pitch cam is translated into rotational motion for the tail.

As the rack is moved back and forth, it rotates the pinion (and therefore the shaft holding the tail) a predetermined amount. This value is determined by the gear relationship between the rack and the pinion and the setting of the pitch cam.

- 9) **Shaft:** The stainless steel shaft translates both the amplitude and pitch motion from the cart to the tail model suspended in the flow tank. It is held in place by a series of bearings in the box beam and on the cart, and is rotated by the pinion at its top end. The bottom end of the shaft is threaded to allow for the attachment of the tail model.
  
- 10) **Mirror Plane:** In order to accurately recreate the force generated by a full tail, using only a half model, a mirror plane is required along an axis of symmetry (ensuring water does not flow through this plane). This was accomplished by simply having the tail move along the top wall of the flow tank. In order to hold and control the tail, a small notch was cut out of the top of the water flume just large enough to fit the shaft and nut holding the tail in place. The shaft (and tail) could therefore move back and forth with only a minor interruption of the mirror plane.
  
- 11) **Box Beam/Force Transducers:** In order to obtain perpendicular force readings of constant orientation, the shaft holding the tail was placed inside a box beam. Forces occurring on the shaft are therefore transmitted into the box beam via the bearings. These forces are then measured using two sets of strain gauges arranged in full Wheatstone bridge configurations (four strain gauges per bridge). These gauges were setup perpendicular to each other and along cut out sections of the box beam (generating a double cantilever beam effect) in order to produce two sets of independent readings, one perpendicular and one parallel to the direction of flow.

It should be noted that while the original design concept called for the use of scotch yokes in generating both the pitch and amplitude motions, the final apparatus made use of cams with solid cranks. While this was done for ease of construction, it did result in the motion of these parameters not being perfectly sinusoidal. A comparison between a standard scotch yoke and crank/slider design is shown in Figure 18. While this difference is expected to be minimal, it may be noticeable in the final force traces and will need to be dealt with during analysis.

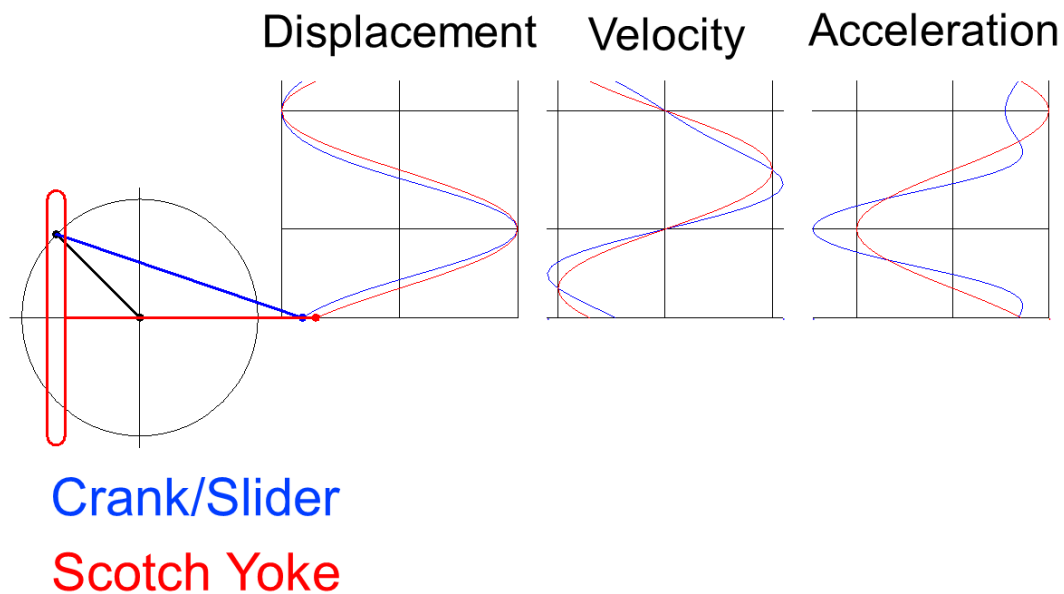


**Figure 18- Cam/Scotch Yoke Comparison:** Comparison of standard scotch yoke and standard crank and slider systems. Figure modified from Wolfram Demonstrations Project.

### Calibration

Once the test apparatus was constructed and functional, but before it was positioned above the flow tank, a series of calibrations were done to determine both force (via the strain gauges) and distance measurements (from the laser sensor).

In order to correlate the voltage readings from the strain gauges with a known force, a string was attached to the end of the shaft (where the tail model would attach) and laid over a pulley. Various weights were then hung off the string, and the resultant voltages were recorded. The output from each set of perpendicular strain gauges was run through its own 2310 Measurement Group amplifier system (gain set at 1000, excitation set at 10V), and fed into the same Biopac/AcqKnowledge data collection system used in the flume calibration (sampling rate was set at 200Hz). For this calibration run, a 10 Hz 2 pole butterworth analog low pass filter was applied at the amplifiers to eliminate AC noise. Forces in the lateral direction (perpendicular to flow) were considered positive if they pushed to the right of the tank, while in the flow direction they were considered positive if they pushed to the back of the tank (Figure 19). This procedure was repeated in both the positive and negative direction for each set of strain gauges. The resultant calibration curves are shown in Figure 20 and 21. As can be seen in these figures, there is a small amount of cross-talk between the perpendicularly oriented gauges. This is most noticeable when an in-flow force is applied, producing a resultant cross-talk of approximately 10% onto the lateral sensor. While 10% is quite small, this result is also further mitigated by the fact that the forces produced in the lateral direction are generally considerably larger than in the in-flow direction. Therefore, the 10% of the in-flow force overlaid on the lateral force will only slightly affect the overall result.

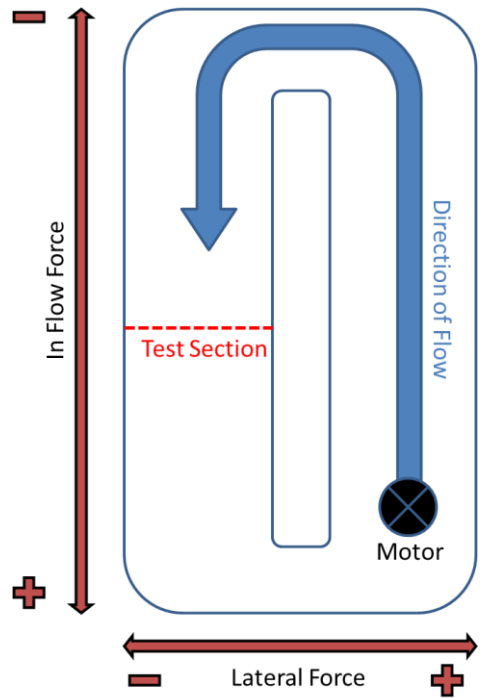


**Figure 19- Force Diagram:** Schematic of the flow tank (top view) showing sign convention for force measurements. In-flow forces are considered positive when measuring drag and negative when measuring lift. Lateral forces are negative when directed to the outside of the test section, and positive when directed to the inside.

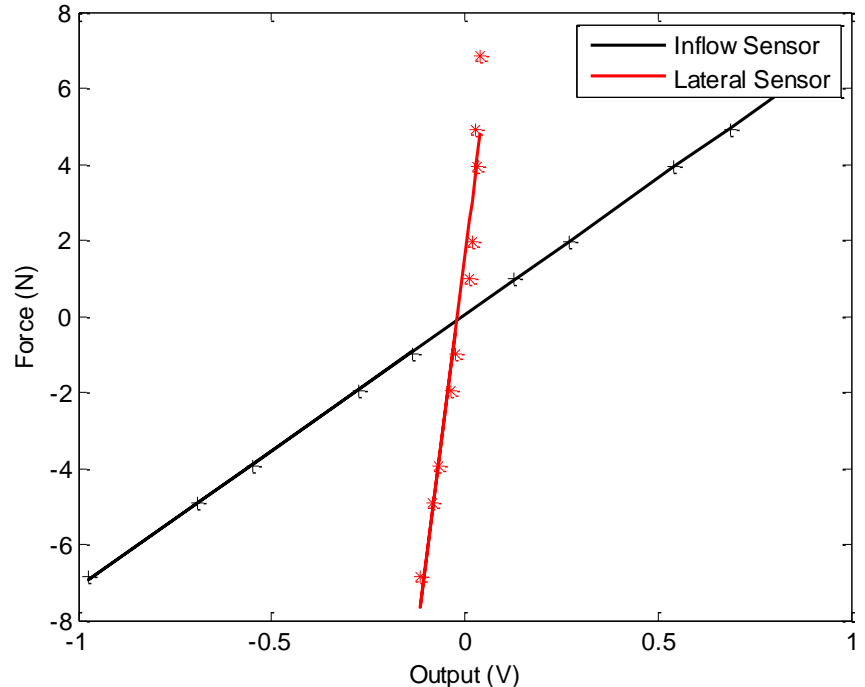


**Figure 20- In-Flow Calibration:** Force/Voltage calibration curves for both lateral and in-flow sensors when forces are applied in the in-flow direction on the test apparatus. In-flow reading indicates calibration curve, while lateral readings indicate the degree of cross talk during testing.

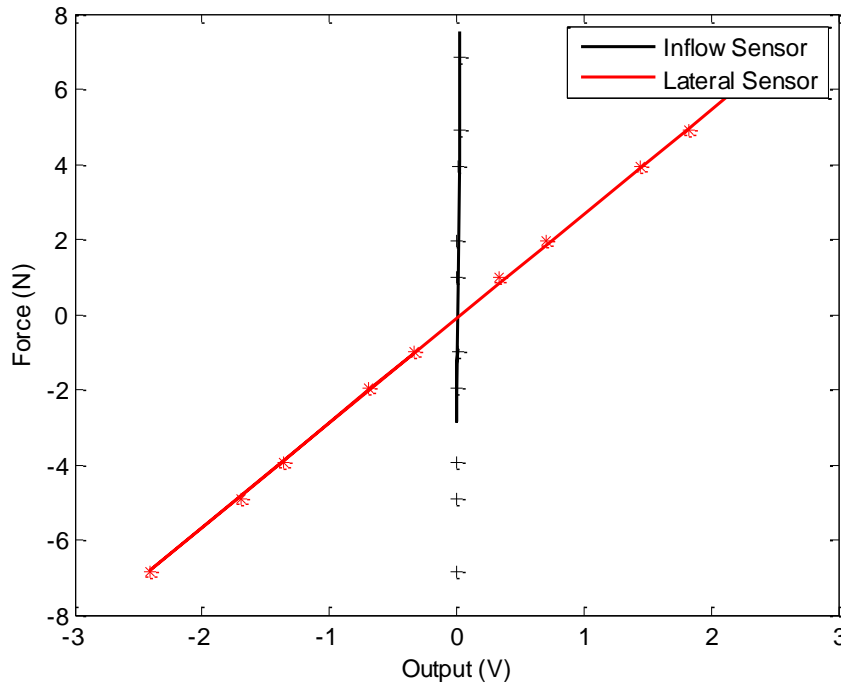


**Figure 21- Lateral Calibration:** Force/Voltage calibration curves for both lateral and in-flow sensors when forces are applied in the lateral direction on the test apparatus. Lateral reading indicates calibration curve, while in-flow readings indicate the degree of cross talk during testing.

The displacement laser arrived pre-calibrated, however a hand calibration was conducted to confirm its accuracy. In order to do this, the laser was placed on a flat surface, and an object was placed at varying distances away from it (between 5-35 cm as per the default sensor range). The output voltage was fed directly into the BioPac/AcqKnowledge system (no amplifier or filtering required). The resultant calibration curve is shown in Figure 22, and falls extremely close to the calibration curve given by the manufacturer (10 volts over the sensor range). As the sensor itself has a far higher resolution than the human eye, it was assumed that this minor discrepancy was due to measurement error in the positioning of the test object, and that the factory calibration represented the more accurate relationship.

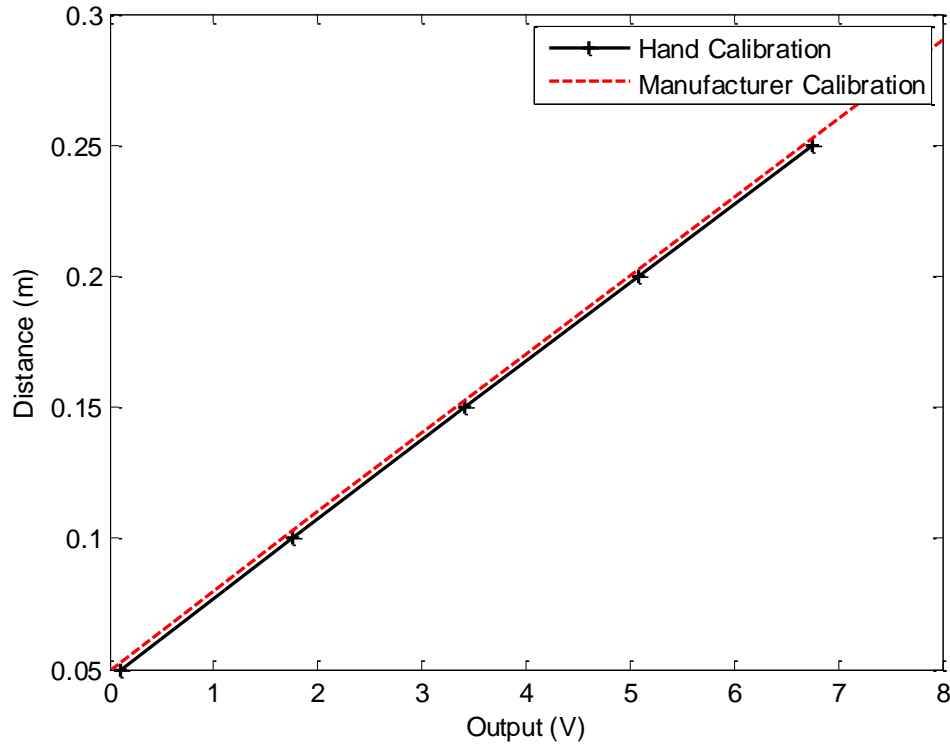


**Figure 22- Laser Calibration:** Calibration curves for laser displacement sensor. Manual hand calibration was almost entirely consistent with the manufacturer’s calibration; therefore the manufacturer’s settings were used.

### **Data Collection /Testing**

After the calibrations of both sets of strain gauges and the displacement sensors were complete, the apparatus could be mounted to the flow tank and testing begun. Data collection during testing was conducted in a similar manner to the calibration. The only major difference between the two methods (before reaching the collection software) was that the low pass filters on the force amplifiers were raised to 100Hz in order to avoid loss of dynamic data.

As the raw signals were collected by the data software, the readings were processed in real time. At each step in the processing the resultant values were recorded, however only the final results were graphed during collection. Firstly all three incoming signals (voltage readings for the two force and one displacement measurements) were filtered using a 2<sup>nd</sup> order digital low pass 25 Hz

filter ( $Q=0.707$ ). This further digital filtering was applied after collection (as opposed to analog filtering at the amplifier) to allow more flexibility in the cutoff value, limit any phase shifting in the filtering, and to ensure the collection of the original data. Next, these filtered readings were converted using their respective calibration curves. Finally, the frequency of the displacement reading was calculated, smoothed (2 second smoothing) and plotted in real time to determine the rotational frequency of the motor (i.e. the tail beat frequency).

With the data collection system setup, testing using the apparatus could now commence. It was at this point that each predefined motion regime was run through twice, once with the tail, and once without. The run without the tail attachment was done in order to get a reading for the inertial forces associated with each setting (all other variables were identical, including water velocity). All runs were conducted in the same manner:

- 1) All sensors were re-zeroed before each run.
- 2) A zero value reading was taken without the flume or apparatus motor running.
- 3) Both motors were started, and the frequencies adjusted to the appropriate values.
- 4) Once readings stabilized, a section of approximately 15-20 seconds was highlighted as the testing region.
- 5) If required, the apparatus motor frequency would be increased for the next set of readings (this only occurred if there were multiple motion regimes whose only difference was in their frequency).
- 6) Steps 4 and 5 were repeated as necessary.
- 7) Both motors were shut off and once readings stabilized a second zero value was taken.

This procedure was repeated 86 times (twice for each of the 43 motion regimes, once with and once without the tail attached). The resultant data from each run were saved as their own data file and stored for further analysis.

Finally, a second set of tests was conducted to determine the static state characteristics of the tail model. This was done in the same manner as the dynamic testing, however the tail location and angle of attack were kept constant through each run. This allowed for the collection of lift and drag forces generated by the tail at three different speeds (0.8m/s, 1.0 m/s and 1.3 m/s) and various angles ( $0^\circ$ ,  $\pm 20^\circ$ ,  $\pm 35^\circ$ ,  $\pm 50^\circ$ ,  $\pm 65^\circ$  and  $\pm 80^\circ$ ).

## **Results/Analysis**

Analysis of the collected data was divided into two areas, the dynamic testing results and the quasi-static testing results. The dynamic testing results were analyzed by determining the mean thrust achieved at each setting and comparing them to the expected overall drag experienced by a similarly sized skipjack tuna swimming at comparable speeds. Those motion regimes that produced biologically relevant forces were then further examined to determine their thrust and drag profiles over a single tail beat. The quasi-static testing analysis was then conducted to determine the static lift and drag characteristics of the foil. These characteristics were used to determine a quasi-static value for the thrust expected at each of the motion parameters. Again, those parameters that yielded biologically relevant forces were analyzed further to determine thrust and lateral force profiles over a single tail beat using quasi-static analysis.

### **Dynamic Testing Results**

#### **Mean Thrust/Drag Values**

In order to determine the mean thrust generation at a given motion regime the following steps were taken:

- 1) A mean zero value was determined for both the run with, and the run without the tail (zero readings were taken before and after each run).
- 2) The mean thrust/drag values were calculated for both the run with and without the tail (this was the mean value of the data once readings had stabilized).
- 3) The mean thrust/drag values were then corrected, by subtracting their respective mean zero values.

- 4) The true mean thrust/drag value generated by the tail was then calculated by subtracting the force generated during the run without the tail (inertial forces generated by the apparatus) from the force generated by the run with the tail (inertial forces generated by the apparatus plus the forces generated by the tail).

A full listing of the forces generated at each motion regime can be seen in Appendix C. This data set was then compared to the overall drag expected by a similarly sized skipjack tuna swimming at this speed. Unfortunately overall drag acting on fish is not commonly available in the literature, as it is extremely difficult to experimentally quantify. Magnuson (1978), however, did conduct a study where the total drag of a 44 cm skipjack swimming at 66 cm/s was determined to be approximately 0.198 N. While calculated by examining different forms of drag over the entire organism, Magnuson does produce an overall coefficient of drag value, and shows that it holds relatively constant over a variety of speeds. Therefore the overall drag force could be expressed as:

$$D = \frac{1}{2} \rho U^2 S C_D \quad \text{Eq. 7}$$

Where D is the total drag force in Newtons, U is the fluid velocity,  $\rho$  is fluid density and S is the total surface area of the organism. By taking the ratio of the drag generated by Magnuson's specimen ( $D_M$ , at a total body length of 44cm and speed of 66cm/s) and our own ( $D_o$ , at a total body length of 57cm and a speed of 100cm/s), the following relationship was made:

$$\frac{D_M}{D_o} = \frac{\frac{1}{2} \rho U_M^2 S_M C_D}{\frac{1}{2} \rho U_o^2 S_o C_D} \quad \text{Eq. 8}$$

This can then be simplified to:

$$\frac{D_M}{D_o} = \frac{U_M^2 S_M}{U_o^2 S_o} \quad \text{Eq. 9}$$

Using isometric scaling the ratio of the surface area for the two organisms is found to be:

$$\frac{S_M}{S_o} = \left(\frac{L_M}{L_o}\right)^2 = \left(\frac{0.44}{0.57}\right)^2 = 0.596 \quad \text{Eq. 10}$$

Similarly the ratio of the square of the two velocities can be found to be 0.436 and the overall expected drag on our specimen can be calculated as follows:

$$D_o = \frac{D_M}{\frac{U_M^2 S_M}{U_o^2 S_o}} = \frac{0.1978}{(0.436)(0.596)} = 0.761N \quad \text{Eq. 11}$$

However, this result should be corrected for the fact that it includes induced drag generated by the caudal fin (approximately 15%), a force already accounted for in the experimental setup. Therefore the true expected drag on our organism (minus the caudal fin) is approximately 0.662 N. Assuming the half tail model produced half of the overall thrust a full tail would produce (0.331 N), there were 4 different motion regimes (18, 23, 24 and 38 as per Appendix C) that were determined to be biologically relevant by producing forces in the range of those expected. These motion regimes were then studied in more detail by examining their thrust and lateral force profiles over a single standardized tail beat.

### Thrust/Lateral Force Profiles

In order to analyze the thrust and lateral force generation over a single tail beat, the following steps were taken:

- 1) The test section of data for a particular motion regime was selected in AcqKnowledge and exported to an excel file which is readable in matlab.
- 2) The data was then run through a 10<sup>th</sup> order low pass Butterworth filter set at 10 Hz or 0.1 of the nyquist frequency as the data was collected at 200Hz (see Figure 23).

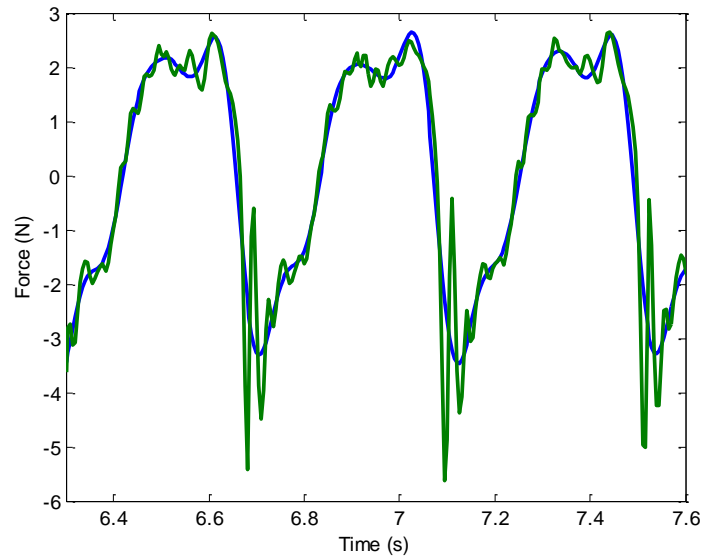


**Figure 23-Data Filtering:** Sample filtered (blue) and unfiltered (green) lateral force data. Data were filtered using a matlab script applying a 10<sup>th</sup> order zero phase shift Butterworth filter.

- 3) 15 consecutive tail beats were isolated and their instantaneous location, lateral force and thrust readings were recorded (minus the mean location reading and zero force readings respectively).
- 4) A standardized mean tail beat was created by averaging each point of the tail beat with its equivalent points in the other 14 tail beats (Figure 24).

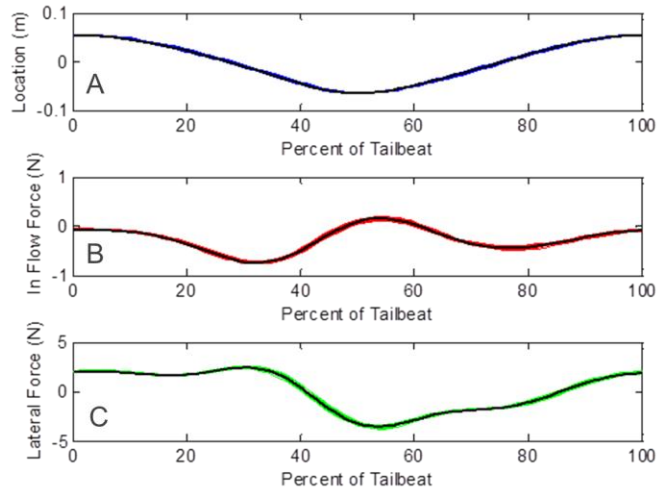


**Figure 24-Standardized Tail Beat:** 15 consecutive tail beats overlaid on each other showing location (A) thrust (B) and lateral force (C). Black lines are average values for all 15 tail beats. The x-axis represents the percent of the tail beat completed. 0 and 100% indicate the tail is at maximum yaw amplitude, while 50% indicates the minimum. The 25 and 75% points indicate the tail is in the middle of the tank.

- 5) Steps 1-4 were repeated for the same motion regimes, but without the tail.
- 6) The resultant waveforms for both the lateral and thrust forces were subtracted from each other ('with tail' minus 'no tail') to generate a true standardized force profile (Figure 25).

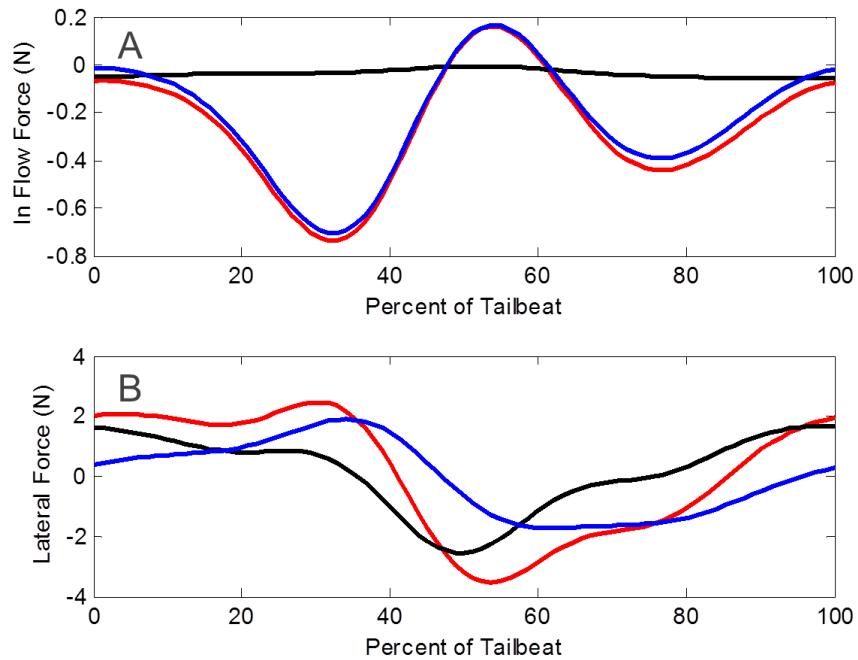


**Figure 25- Normalized Tail Beat:** Thrust (A) and lateral forces (B) over a standardized tail beat, for a run without a tail (black), with a tail (blue) and the difference of the two (red).

This method also allowed for the calculation of the mean lateral force generated over a tail beat (expected to be zero due to symmetry) and a mean for the absolute value of the lateral force (which represents the total lateral force generated by the tail). A full listing of the lateral force and thrust profiles for all 4 relevant motion parameters can be seen in Figure 29 and is summarized in Table 2.

At this point, it can be seen in Figure 25 neither the lateral, nor the thrust forces generate a symmetrical profile as might be expected due to the symmetry of motion. This effect is likely due to the slight asymmetry associated with using a rotating cam as opposed to a scotch yoke, as well as asymmetry in the tail itself, and will be addressed in the analysis section titled “Symmetry Analysis.”

### Power and Efficiency

A common way of measuring efficiency for a propeller like system is to calculate what is known as its Froude efficiency ( $\eta$ ). This is essentially simply the ratio of output power ( $P_{out}$ ) over input power the system ( $P_{in}$ ):

$$\eta = \frac{P_{out}}{P_{in}} \quad \text{Eq. 12}$$

Instantaneous power can be calculated as the force exerted in a direction multiplied by the speed of travel in that direction at any given point in time. As the swimming speed in our case is constant  $P_{out}$  is simply the mean force output per tail beat ( $F_{Flow}$ ) in the direction of travel multiplied by the swimming speed ( $U$ ):

$$P_{out} = F_{Flow}U \quad \text{Eq. 13}$$

$P_{in}$  on the other hand is considerably more complicated. This is due to the fact that it consists of two forces (lateral force, and torque force), and that neither of these have a velocity constant with time. Therefore, as described in Anderson et al. (1998), in order to calculate the power input per tail beat an integral approach has to be adopted:

$$P_{in} = \frac{1}{T} \left( \int_0^T F_{Lat}(t) \frac{dlat}{dt} dt + \int_0^T F_{\theta}(t) \frac{d\theta}{dt} dt \right) \quad \text{Eq. 14}$$

Where  $F_{Lat}$  and  $dlat$  are the force and displacement in the lateral direction, and  $F_{\theta}$  is the torque. Unfortunately as there were no torque measurements made in this study, only a proxy value of efficiency could be made. As this assumes the torque values are negligible compared to the output and lateral forces, any values are likely overestimations of the true efficiency. These calculations were made using a matlab script for the four biologically relevant regimes and their results can be seen in Table 2.

### Repeatability

The repeatability of this method was assessed by repeating two motion regime tests (numbers 23 and 38 as per Appendix C) five separate times. In order to do this, runs both with and without the tail were conducted, and the mechanical linkages on the test apparatus were adjusted and reset between each run. The repeatability of the measurements both with and without the tail seemed to hold surprisingly steady with a standard deviation of about 0.023 N in both cases. With the tail attached, these standard deviations represented only approximately 8% of the mean test value. These values were considerably higher for when the tail was not attached (79%), but this was due to the decrease in the mean test value without the tail, not an increase in the standard deviation.

By comparison, a second set of tests were conducted using the same regimes, but with the tail purposefully offset by  $10^\circ$  in each direction (the sin wave of the tail motion oscillated around  $\pm 10^\circ$  instead of  $0^\circ$ ). This small change decreased the thrust production in regimes 23 and 38 by an average of 66%.

As the error associated with repeatability was so small, especially when compared to the error associated with a minor (yet purposeful) offset in the pitch angle, it was deemed that the methodology used in testing was repeatable, with results achieving a high level of precision.

### **Quasi-Static Testing**

#### **Coefficient of Lift/Drag**

The static state lift and drag data was extracted and averaged in a similar manner to the mean thrust values conducted in the dynamic testing. Using these values it was now possible to determine the coefficients of lift ( $C_L$ ) and drag ( $C_D$ ) of the foil as a whole. These coefficients are essentially non-dimensionalized measures of how much lift or drag a foil generates at a particular angle, normalized for fluid speed/density and foil size:

$$C_L = \frac{L}{\frac{1}{2}\rho V^2 S_c} \quad \text{Eq. 15}$$

$$C_D = \frac{D}{\frac{1}{2}\rho V^2 S_c} \quad \text{Eq. 16}$$

Where L and D are the lift force and drag force in Newtons respectively, V is the fluid velocity,  $\rho$  is fluid density and  $S_c$  is the planform area of the foil.

Using these equations the two coefficients were determined for each angle and flow speed tested.

As the coefficients are normalized for velocity, and the tail model is considered symmetrical,

variations due to velocity and direction of angle of attack (i.e.  $+10^\circ$  versus  $-10^\circ$ ) were considered negligible, allowing for the coefficients to be grouped by angle of attack (Figure 26). It should be noted that some deviation from the assumed perfect symmetry of the foil can be seen in the plot as the coefficient of lift does not reach zero at a  $0^\circ$  angle of attack. However this is a small deviation due to the curve in the tail specimen and is assumed to be negligible.

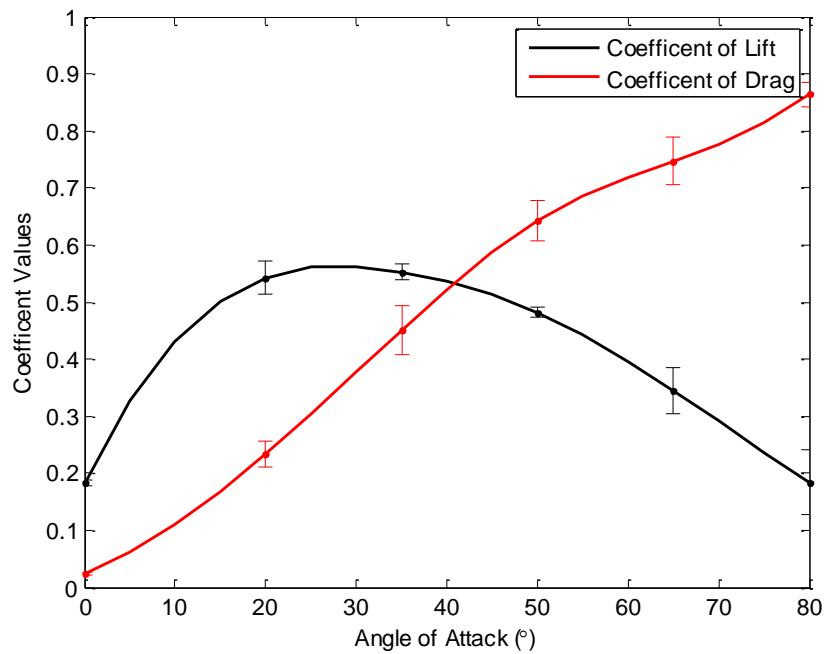


**Figure 26- Coefficients of Lift and Drag:** Coefficient of lift and drag values for the model tail at varying angles of attack under static conditions. Data was collected at both positive and negative angles at varying speeds (0.8 m/s, 1m/s and 1.3 m/s).

Similarly a polar diagram outlining the relationship between the two coefficients was also created (Figure 27).

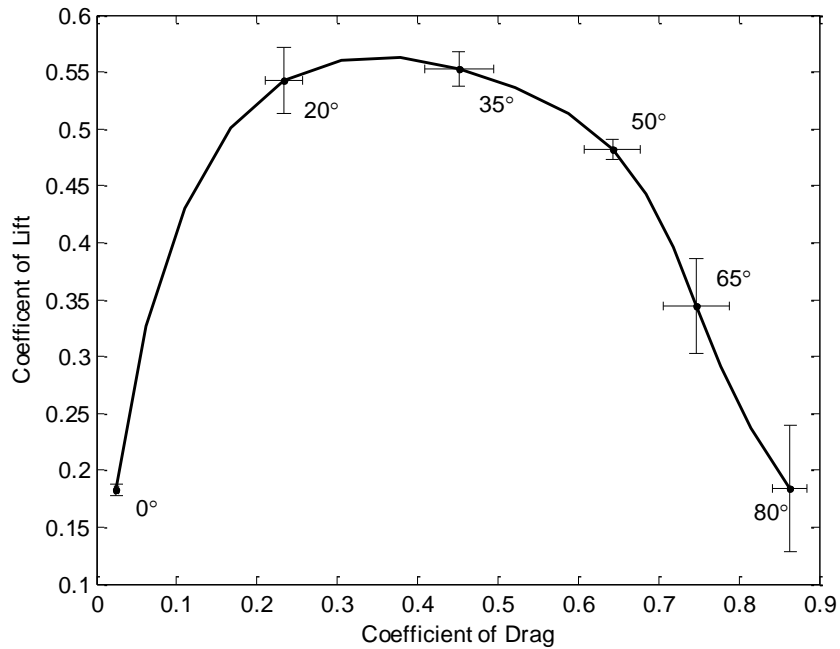


**Figure 27- Polar Diagram:** A polar diagram describing the lift and drag characteristics of the tail model under static conditions. Left side of the plot indicates an angle of attack of  $0^\circ$ , increasing steadily to  $80^\circ$ .

The repeatability of this method was examined by re-testing a single angle and orientation three times at both the extreme left and right of the test section (60mm to either side of the center of the tank). At each test location the standard deviation between runs was always less than 2.5% of the measured value for both drag and lift. When the values collected at different locations were compared however, the mean difference between the left and right side of the test section rose to nearly 19% of the mean value. This asymmetry, which is likely due to the skewed flow profile, could be the cause of error in the quasi-static static analysis and will be addressed in the section titled Symmetry Analysis (below). It should be noted that the actual quasi-static testing was conducted at 30mm to either side of the center of the tank (as opposed to the 60mm at which the repeatability testing was done), so errors associated with this repeatability test are likely somewhat overstated.

## Mean Thrust Values

Using these relationships, it was now possible to create a matlab program to predict the thrust and drag production of each set of motion parameters using a quasi-static analysis method. For each motion parameter a standardized tail beat was mathematically generated. Then each tail beat was divided into a hundred instantaneous points. At each point the instantaneous local velocity and corresponding angle of attack were determined. This allowed for the calculation of the coefficients of lift and drag forces via Figure 27 which could, in turn, be converted to thrust/drag and lateral forces relative to the free stream velocity (Figure 28). The mean value of these forces over an entire tail beat are shown in Appendix C.

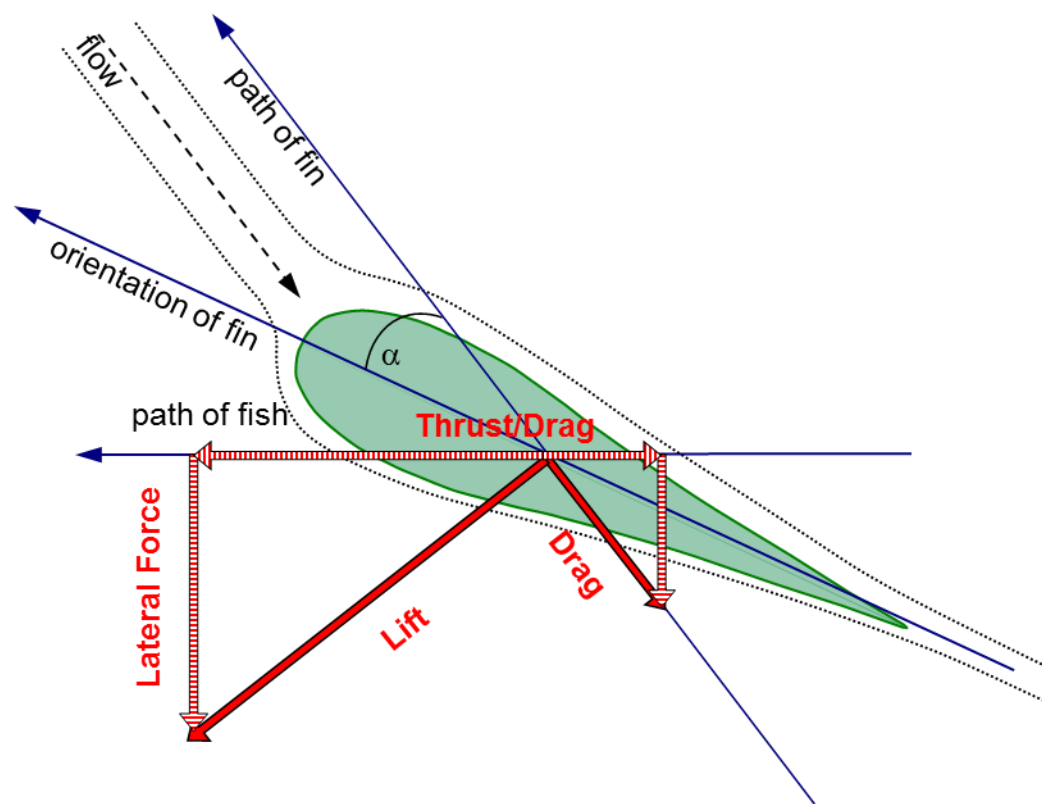


**Figure 28- Quasi-Static Analysis:** The quasi-static approach is used to determine the lift and drag relative to the direction of instantaneous flow (red arrows). These forces are then broken down to their component vectors of thrust/drag and lateral force relative to the path of the fish (striped arrows).

### Thrust/Lateral Force Profiles

Similarly, these calculated instantaneous forces could be plotted versus their location in the tail beat in order to show the expected thrust/drag and lateral force profiles. This was done for the four motion regimes that were deemed to be biologically relevant and can be seen in Figure 29. Much like the dynamic analysis, this process was also used to calculate the mean lateral force as well as the mean of the absolute value of the lateral force (Table 2).

As can be seen in Figure 29, all calculated profiles have a noticeable and sudden change at regular intervals. It should be noted that this is an artifact in the data due to the error associated with calculating the lift coefficient, specifically the fact that the coefficient of lift is not zero at zero degrees. Therefore as the local angle of attack approaches  $0^\circ$  from one direction, the coefficient of lift will approach approximately 0.2. The moment the angle of attack passes  $0^\circ$  the coefficient of lift will jump to 0.2, but in the exact opposite direction. This sudden change causes these ‘dips’ in force production, but are generally assumed to be negligible.

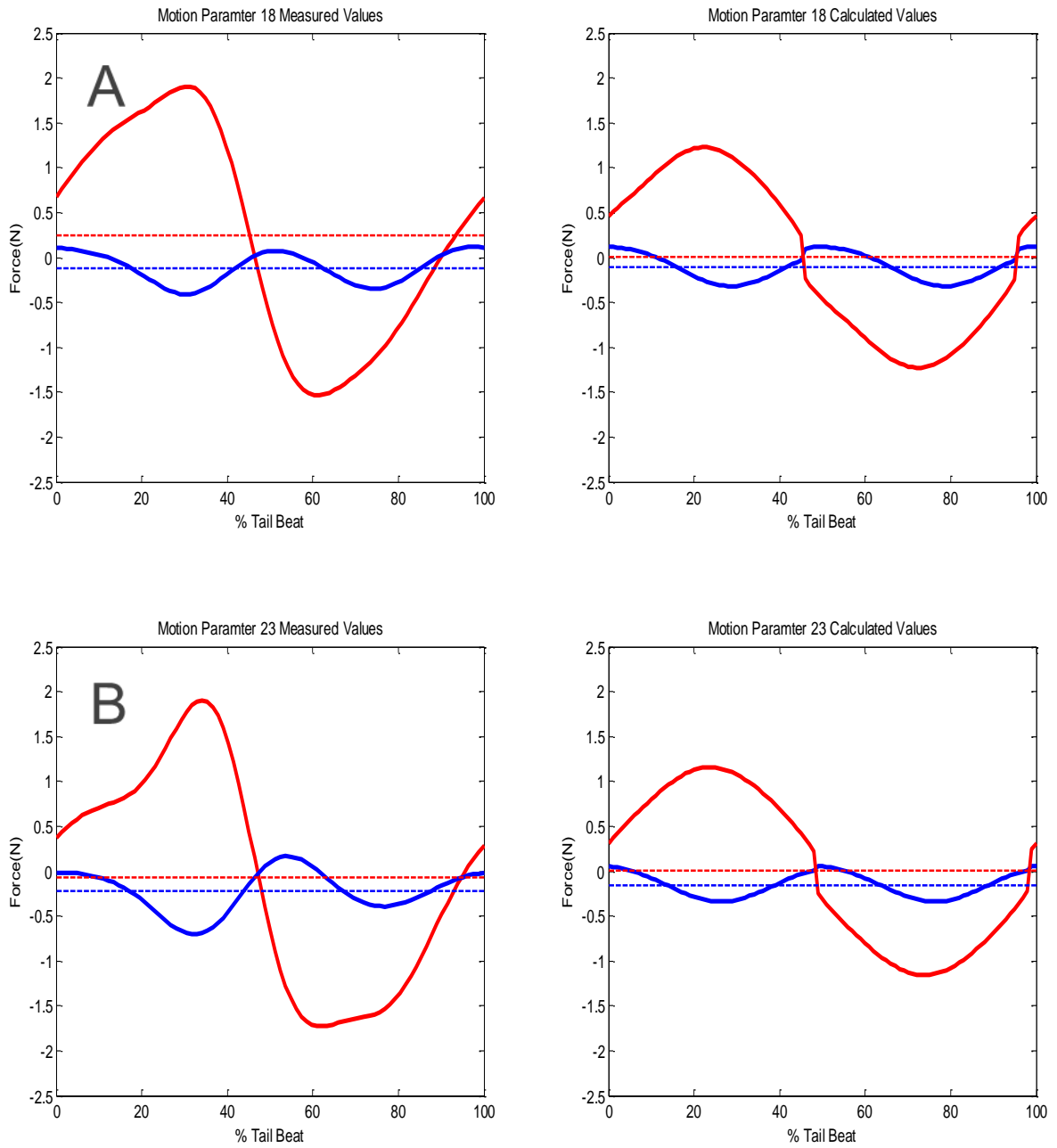


**Figure 29A- Biologically Relevant Flow Profiles:** A comparison of measured and calculated force profiles for each of the biologically relevant regimes. In flow forces are shown in blue, while lateral forces are shown in red. Dashed horizontal lines indicate mean values. Plots A, B, C and D represent regimes 18, 23, 24 and 38 respectively.

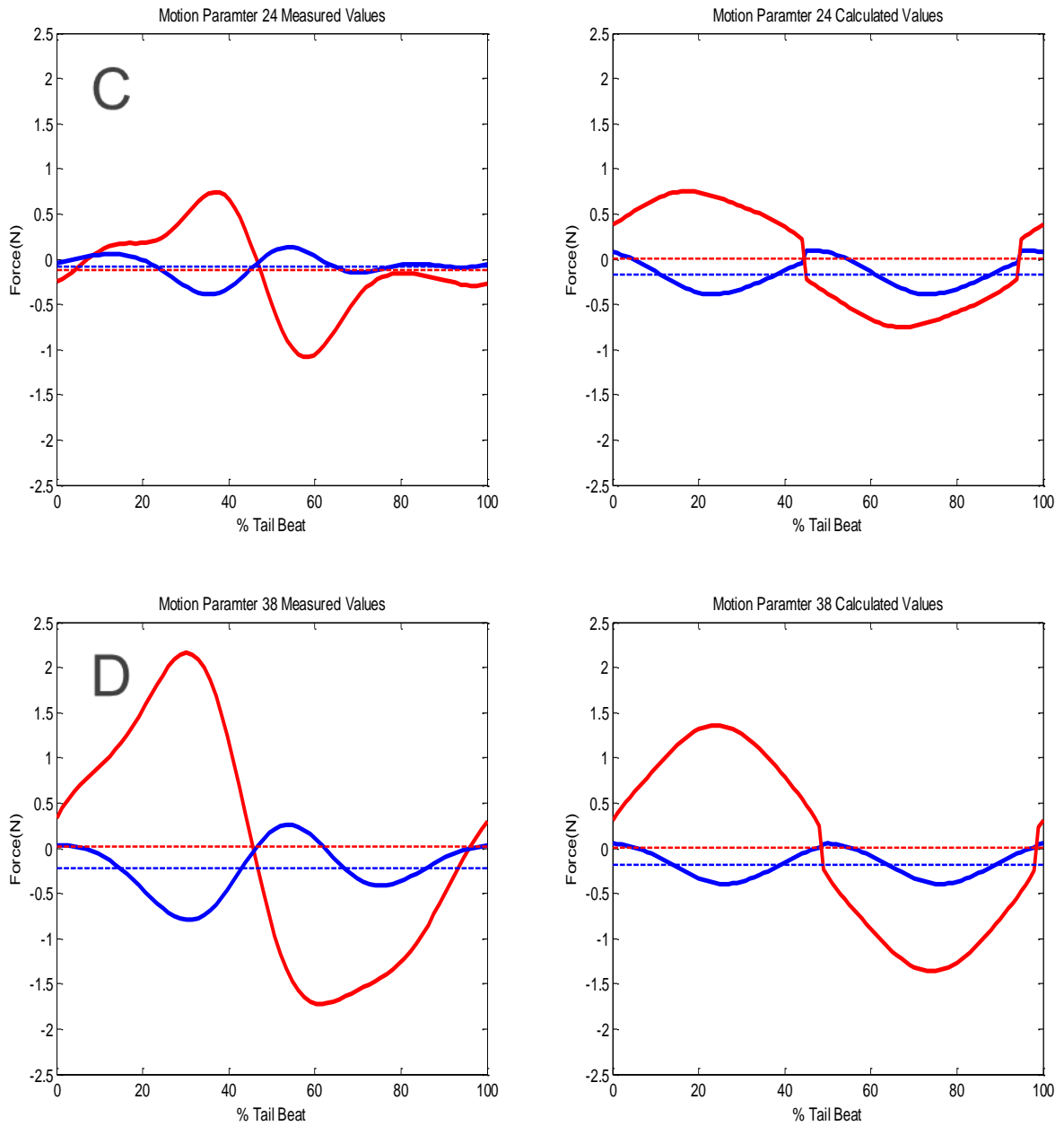


**Figure 29B- Biologically Relevant Flow Profiles:** A comparison of measured and calculated force profiles for each of the biologically relevant regimes. In flow forces are shown in blue, while lateral forces are shown in red. Dashed horizontal lines indicate mean values. Plots A, B, C and D represent regimes 18, 23, 24 and 38 respectively.

Regime	Mean Measured Thrust (N)	Mean Calculated Thrust (N)	Mean Measured Lateral Force (N)	Mean Calculated Lateral Force (N)	Mean Measured Absolute Lateral Force (N)	Mean Calculated Absolute Lateral Force (N)	Mean Angle of Attack, $\alpha$ (°)	Measured Thrust Coefficient, $C_T$	Froude Efficiency, $\eta$ (%)
18	-0.125	-0.116	0.247	0.005	0.884	0.832	17.5	0.116	16.7
23	-0.214	-0.157	0.064	0.003	0.770	0.799	15.9	0.199	30.1
24	-0.111	-0.160	0.120	0.004	0.176	0.538	6.6	0.103	34.7
38	-0.213	-0.182	.0241	0.003	0.853	0.9144	18.4	0.198	24.6

**Table 2 - Summary of Results:** Summary of key force values associated with each of the biologically relevant motion regimes.

### **Symmetry Analysis**

As can be seen in Figure 29 the measured force profiles are not symmetrical about the midpoint of the tail beat. Symmetry would typically be expected, as for the first 50% of the tail beat, the tail is moving in one direction across the flow tank, and for the second 50% it is moving in an identical fashion back. There are three major methodological reasons why this asymmetry is believed likely to occur. Firstly as noted in the quasi-static analysis, the tail half being studied is not perfectly flat, as there is a slight curve in one direction. This should lead to differences in force generation depending on the orientation of the tail (i.e. a foil at  $+10^\circ$  will generate slightly different forces than a foil at  $-10^\circ$ ). Secondly, as discussed earlier the use of cams instead of scotch yokes to generate changes in amplitude and pitch mean that these motions will deviate slightly from a perfect sinusoidal form. This would affect the instantaneous velocity of the foil and therefore change the force it generates. The third possible factor is the asymmetry of the flow profile in the test section of the tank. This final factor however is likely surprisingly small, simply based on the physical location of the tail when it is generating thrust. As can be seen in

Figure 29, thrust is almost exclusively generated when the tail is at the center of the tank (the 25% and 75% point of the tail beat). Therefore the free stream velocity at these two points should be nearly identical. Furthermore for the thrust generating regimes (where pitch leads yaw by nearly  $90^\circ$ ) the greatest differences in free stream velocity would occur when the tail was essentially parallel to the flow. For these reasons, only the effects of the first two factors were examined to help determine if they significantly altered the force profiles seen in the experiment (this was done on data from flow regime number 23).

Firstly, the experimentally collected data were modified to force symmetry about the halfway point of the tail beat. This was done assuming that the factors causing asymmetry were themselves in fact symmetrical. For example, due to the cam/scotch yoke issue, the tail might move slightly faster going in one direction as opposed to the other (i.e. the velocity at 25% of the tail beat might be slightly faster than the velocity at 75% of the tail beat). However the expected velocity from a perfect sinusoid should be the average of the two. Similarly a small deviation from foil symmetry might increase thrust slightly going in one direction, but it could be expected to decrease thrust going in the other direction by virtually the same amount. It was with this in mind that a script was generated to average the two halves of the standardized thrust profile. For example, the point marking 1% of the tail beat was averaged with the point marking 51% of the tail beat, and the new value was used for both points. Similarly the points marking 2% and 52% were averaged, 3% and 53%, etc., up to 50% and 100%. The results of this modification can be seen in Figure 30.

It could be asked, however, how much of the symmetry shift seen is due to the cam/yoke factor versus the curve in the tail shape. In order to address this, a second data modification was done, this time to the calculated thrust profile (obtained using the coefficient of lift and drag).

Essentially the same procedure was followed for creating the profile as before, but this time

instead of using a sinusoid function to determine the instantaneous location and velocity of the foil, the actual cart location and velocity was used (imported from the experimentally collected laser data). The results of this modification can also be seen in Figure 30. A comparison of these to modified data sets can be seen in Figure 31.

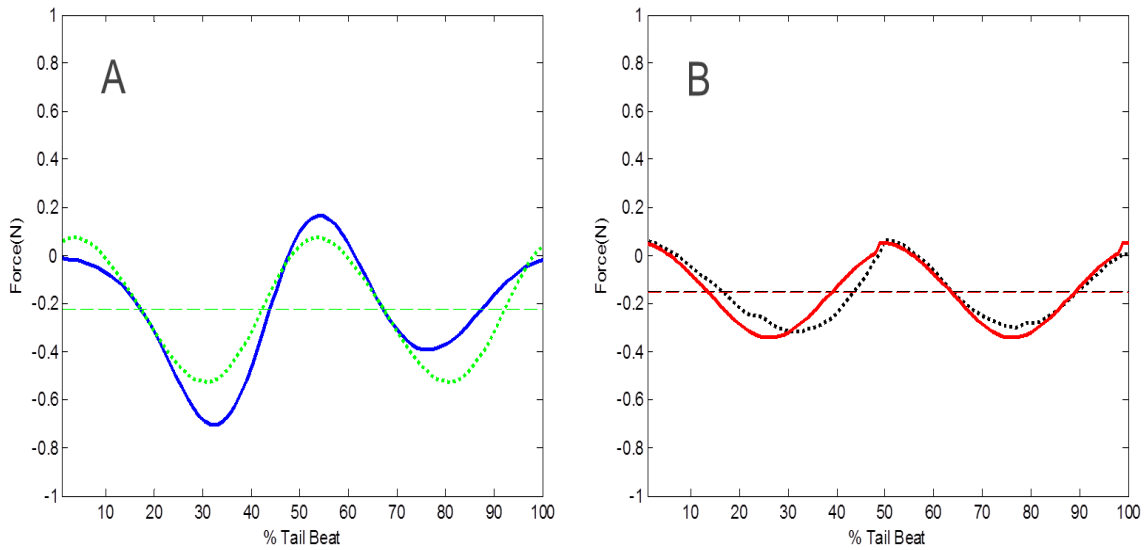


**Figure 30- Symmetry Analysis:** Measured (A) and calculated (B) thrust force values before and after symmetry modifications. Solid lines indicate original values, dotted lines indicate modified values and dashed horizontal lines indicate mean values.

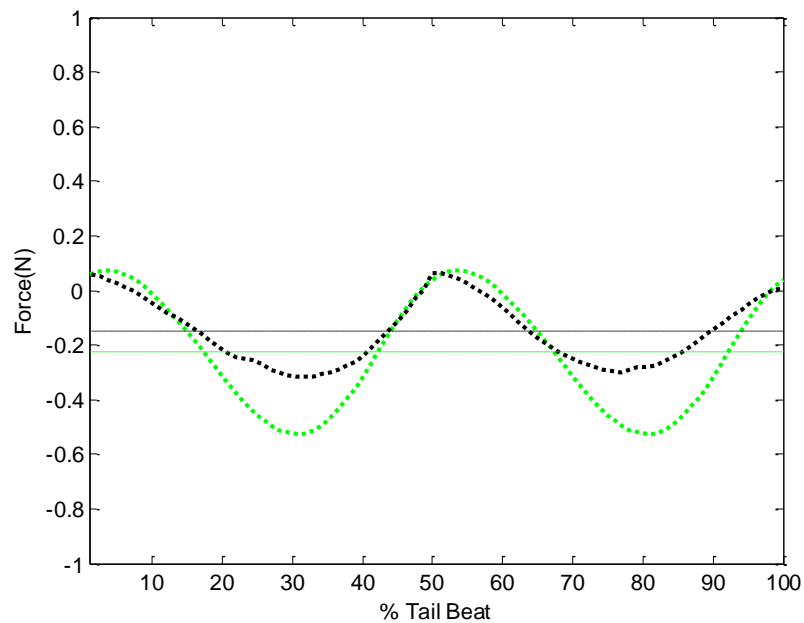


**Figure 31- Symmetry Comparison:** Comparison of modified measured (green) and modified calculated (black) thrust force values for regime 23. Horizontal dashed lines indicate mean values.

By comparing the effect these modifications had on their respective data sets, several points can be made. To begin with, it can be seen that correcting for the asymmetry in motion alone (by modifying the calculated thrust profile), had only a minimal effect. Correcting for both the asymmetry in the tail and the motion, however, had a pronounced effect. It could therefore be concluded that the asymmetry caused by the cam/yoke design is in fact quite minimal. Similarly it could be deduced that the majority of the asymmetry is in fact due to the asymmetry in the tail itself. Furthermore, as a point of clarification, it should be noted that neither of these modifications affected the average thrust produced over a tail beat, and therefore asymmetry in the experimental design can be ruled out as the cause for the difference between experimental and calculated values.

## **Discussion**

A great deal of data was collected in the course of this study, and the possible analysis and interpretations thereof are seemingly limitless. It was therefore decided that the most appropriate method of dissecting and processing this data was to return to the hypothesis set out at the beginning of this study as a guide. While it is possible that further analysis could be done on this data and new relationships or behaviors brought to light, it is the primary goals of this study which must be analyzed in the greatest detail:

### **Hypothesis 1: Thrust generation will occur only under a specific range of tail motion parameters:**

Result: Experimental data supports the hypothesis.

By examining Appendix C it is immediately apparent that only a small fraction of the tested motion regimes can produce any amount of forward thrust, and only a still smaller subset of those can be considered biologically relevant.

With so many variables and such a small sample of relevant regimes, it is impossible to conclusively state which motion parameters have the greatest effect. Furthermore, the precise values or ranges of these parameters that would generate peak thrust can not be well defined. However some general trends can be seen, as listed below. These trends will be compared to both in vivo observational data (Parry, 1949; Fierstine and Walters, 1968; Magnuson, 1978) and in vitro experimental data already present in the literature (Anderson et al., 1998).

While these comparisons are insightful, they should also be taken with a degree of caution. With regards to the observational data, often it is somewhat dated and was not collected with the benefit of modern motion analysis techniques, leaving the degree of accuracy in question.

Additionally, the exact behavior of the specimen at the time of observation (i.e. accelerating, cruising, breaking, etc.) is not always clear, leaving the door open for possible misinterpretation.

The experimental analyses on the other hand often lack an appreciable level of bio-fidelity.

Anderson et al. (1998), for example, is a highly cited source in such matters, as they thoroughly investigated peak efficiencies of pitching and oscillating foils. Their experimental setup however, was not intended to mimic a caudal fin in either form (i.e. no sweep back angle, constant cross section, etc.) or function (i.e.  $H_o$  values were always less than 1.0). Furthermore, while that particular investigation was attempting to resolve what regimes produce peak efficiency, there is no guarantee that in vivo specimens actually swim at peak efficiency or thrust (to be discussed in Hypothesis 6). With that in mind however, several of these comparisons can be quite insightful when studying the parameter trends required to produce thrust.

- 1) **Phase Lag ( $\phi$ ) needs to be relatively high:** Three of the four relevant motion regimes (including the two highest recorded thrust values) were at the highest tested phase lag of  $80^\circ$ . The other relevant regime was at the next highest tested setting of  $60^\circ$ . This indicates that the foil is at its lowest pitch angle when it is very close to its highest amplitude and vice versa. This also indicates that the pitch angle is at its greatest when the tail is very near to its maximum lateral velocity.

This phase shift between yaw amplitude and pitch angle (shown in Figure 32), is somewhat intuitive from a quasi-static perspective. Primarily, if the two measures were in phase (zero pitch angle at minimum displacement), then the increased velocity from the lateral motion would only have the effect of creating a drag force against the motion of the tail. By increasing the pitch angle at this point slightly, it will not only reduce the drag, but also induce localized lift by providing a small

angle of attack. This lift would have components both in the lateral and forward (thrust) directions.

Furthermore, these values are supported by previous experimental and observational work. Anderson et al. (1998), indicating that peak thrust efficiency should occur at 75°. Parry (1945) also indicated that the phase lag for bottlenose dolphins was approximately 90° out of phase.

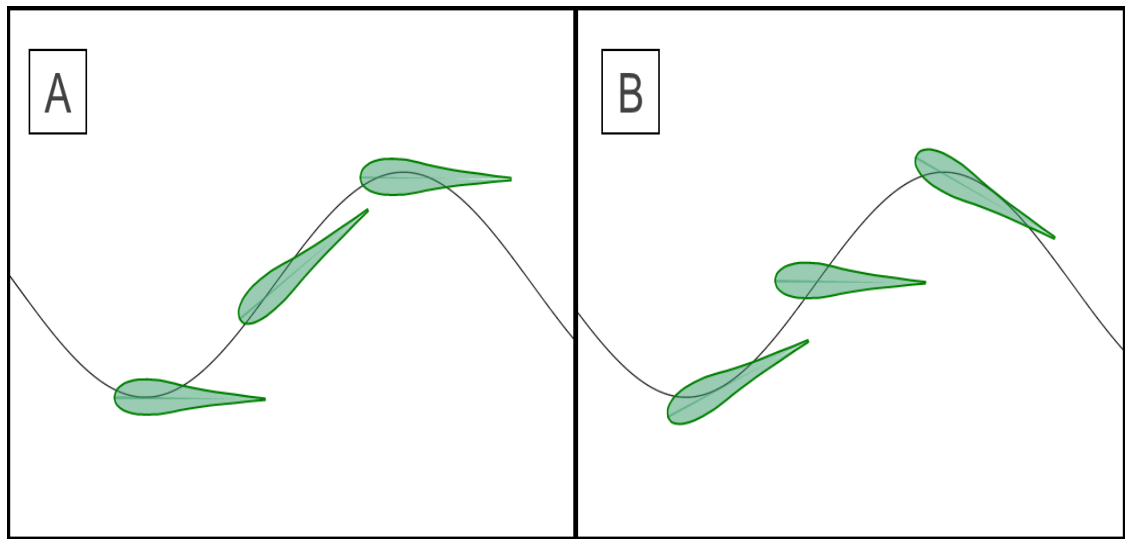


**Figure 32- Phase Lag Diagrams:** Diagrams showing the effect of phase lag on angle of attack relative to yaw amplitude. A phase lag of approximately 90° is shown in Figure A, while a phase lag of 0° is shown in Figure B.

- 2) **Nominal Pitching Angle ( $\theta_0$ ) needs to be relatively low:** Again, three of the four relevant regimes shared a single value for this parameter (20°), while the fourth was at the next lowest tested value of 35°.

While less intuitive, this again can be interpreted via a quasi-static approach. Ideally the instantaneous angle of attack should be relatively small to generate peak lift (approximately 28° according to Figure 26). While an angle of attack too high will cause lift to be reduced, there is also the possibility of achieving a negative angle of attack (if the pitching angle is too high), thereby creating lift with a component in the drag

direction. Unfortunately, the angle of attack is determined by both the instantaneous velocity of the tail and pitch angle, and therefore it would be misleading to study one variable without the other. However the results do indicate that over the regimes (and therefore the lateral velocities) tested, a small pitching angle is the most appropriate for generating thrust.

Additionally the average angle of attack, for thrust generating regimes ( $6.6^{\circ}$ - $18.4^{\circ}$ ) seems to fall in line with Anderson et al. (1998), as well as values from Fierstine and Walters (1968) of  $15^{\circ}$ - $25^{\circ}$  and  $29.2^{\circ}$  respectively. It should be noted however that similar angle of attacks are also present in drag producing regimes, so while an angle of attack inside this range may generate thrust, it does not guarantee it.

3) **Normalized Yaw Amplitude ( $H_o$ ) needs to be large:** This result is indirectly implied by the previous results stating that the phase lag should be high and that the pitching angle should be quite small. This is due to the fact that one of the major factors in determining whether to test a regime or not was based on its tail tip amplitude matching real life values. As the first two results indicate that the tail tip amplitude will typically remain close to the pitching axis amplitude (particularly at peak excursions), the pitching axis amplitude must therefore account for virtually all of the tail tip amplitude. It is therefore not surprising that all thrust generating regimes had a yaw amplitude ( $A_o$ ) at the maximum tested value (60 mm).

These results (which equal approximately 10.5% of full body length) fall well within the range observed by Fierstine and Walters (1968) (7.5-16% of BL), however they are considerably larger than those obtained at peak efficiency by Anderson et al. (1998), ( $H_o$  of 2.8 versus 0.75). This major discrepancy with Anderson et al., is likely caused by the fact that this study examined biologically relevant regimes ( $0.7 < H_o > 2.8$ ), while the

previous study explored peak efficiency regimes ( $0.25 < H_o < 0.75$ ). It is interesting to note however that both studies found the best operating conditions to be at the highest yaw amplitudes tested.

4) **Within the range given, frequency (f) does not appear to be a determining factor:**

With such a small range of tested frequencies, it is difficult to make any conclusions about the effect of frequency on force production. It does appear however that if all other criteria are met, any frequency within the tested range will produce thrust to some degree. Whether or not this corresponds to peak efficiency, however, is a different matter (see Hypothesis 6).

**Hypothesis 2: Thrust generation will be close to, but slightly less than the total drag expected on the fish:**

Result: Experimental data supports the hypothesis.

As was described in the dynamic testing analysis, the expected drag on a skipjack tuna of 57 cm traveling at 1 m/s is approximately 0.662 N. For steady swimming therefore, it would be expected that each half of the caudal fin (as modeled by the apparatus) would produce 0.331 N.

In actual fact, the highest force production measured was 0.214N, equivalent to roughly 65% of expected thrust. This comparison can also be made via the coefficient of thrust, where the expected value was determined to be 0.307, while the highest experimental value was found to be 0.198. As expected, the experimental thrust is lower than the predicted drag, but the precise factors causing this discrepancy are not well known. Some possibilities include:

- 1) **Error in drag calculations:** Firstly it should be stated that the overall coefficient of drag was based on calculations summing expected drag for different parts of a fish body. While these calculations did take into account form and friction drag (as well as induced drag where appropriate), there is still room for a fair amount of uncertainty in these calculations. Furthermore, in calculating the overall drag on our larger test specimen, it was assumed that the scaling effect would be isometric. While this is likely true in a general sense, it is likely not a perfectly accurate assumption. Finally, a large portion of overall drag is assumed to be due to gill resistance. As tunas are ram ventilators, they swim with their mouth open to allow water to flow over their gills. While this can generate a great deal of drag (approximately 17% of total drag according to Magnuson, 1978), this value would obviously be dependent on the gape angle and swimming velocity. As tuna tend to decrease the gape angle of their mouths as their swimming speed increases, there is the possibility that this drag source is quite variable. In total, the combined sources of uncertainty in this analysis are significant, and therefore values attained should not be taken as definitive. While they are likely accurate on an order of magnitude scale, the exact accuracy is at this point unknown.
- 2) **Non-caudal thrust generation:** While the great majority of thrust in thunniform propulsion is generated by the caudal tail, amputated tunas can still produce approximately 10% of their normal thrust (Fierstine and Walters, 1968). While this is a small value, it would represent a sizable amount of the difference between predicted drag and measured thrust.
- 3) **Upstream flow conditioning:** Fish are known to use upstream flow conditions to their advantage. This could be something as simple as finding a path of least resistance (slowest incoming flow), or as complicated as positively interacting with disturbances in

the flow (i.e., rocks or even other fish). Triantafyllou, 2002 showed that the coefficient of thrust for a flapping foil could range widely (from below 0.1 to above 0.6) based simply on its relative location to an upstream bluff body. It is possible that the tuna body itself (anterior to the peduncle) could have a similar effect, possibly allowing vortices shed by upstream morphological features (such as the dorsal or anal fins), to positively interact with the caudal fin (Lauder et al., 2007). Furthermore these upstream features could have other positive effects such as redirecting water flow, or reducing boundary layer separation.

- 4) **The ideal flow regimes may not have been tested:** While the regimes tested consisted of discrete points for each parameter, the true range of possible regimes is in fact a continuum of parameter values. The fact that there are four input parameters (five if one were to consider the pitch axis location) and that these parameters are often obscurely related to each other makes this continuum difficult to define explicitly, however it does consist of continuous not discrete values. It is quite possible and in fact likely that the regime producing peak performance (whether measured in thrust production or efficiency) was not tested. Anderson et al. (1998), showed that at peak efficiency (approximately 87%) a flapping foil could reach thrust coefficients of over 0.5 without any upstream conditioning. It is possible that a more refined range of motion regimes will reveal increased thrust for the current model.

**Hypothesis 3: Quasi-static modeling will under predict thrust generated by the tail:**

Result: Experimental data is inconclusive with regards to the hypothesis.

When the results of the expected calculated thrust values (via quasi-static analysis) are compared to the experimentally measured thrust values several observations can be made (Figure 33).

Firstly, over the entire range of tested motion regimes, the calculated values do a surprisingly good job of predicting thrust, with slightly over 91% of the variation in measured values being accounted for by the calculated values. That being said, they also under-predict the thrust by nearly 53%. This under-prediction was expected, as a quasi-static approach only takes into account the resistive forces of the fluid and ignores the inertial forces. So for example, using quasi-static methods, a foil will be producing the same amount of lift and drag at two different points assuming that they share the same fluid velocity and angle of attack. A more realistic model (such as reactive modeling) takes into account those forces that are dependent on the rate of change of the velocity and the associated virtual mass (Webb, 1975).

Unfortunately this relatively predictable relationship seems to fall apart over the smaller range of biologically relevant regimes ( $R^2=0.331$ ). It is quite likely that this weak relationship is due to the extremely small sample size, however with the possible range of biologically relevant thrusts being quite small, it is unclear how strong the relationship will be even with additional tests.

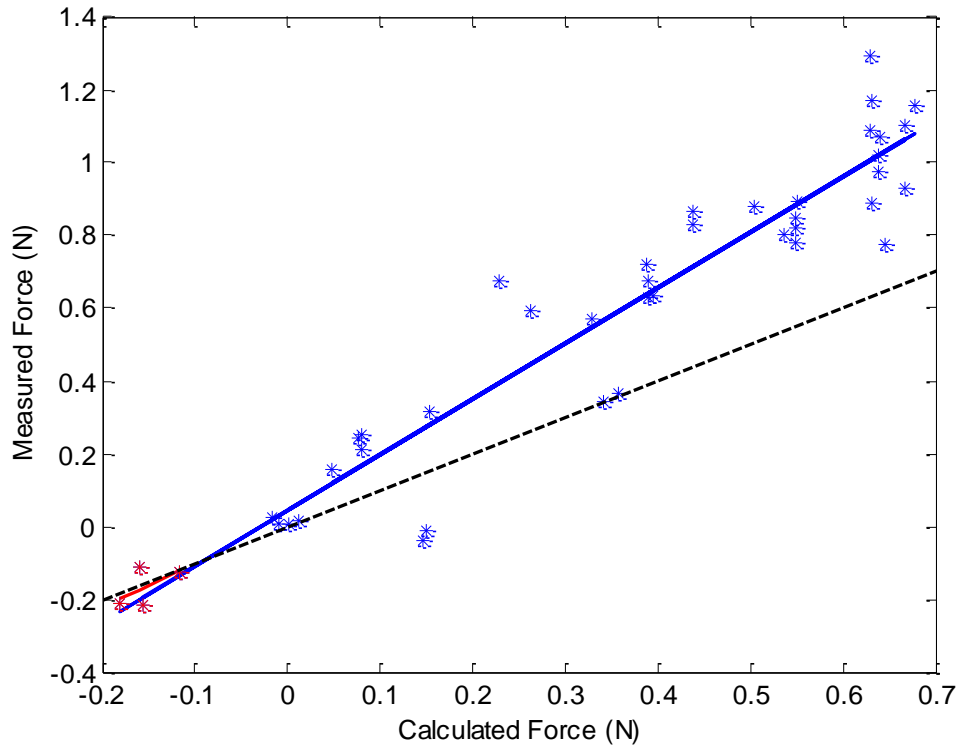


**Figure 33- Measured vs. Calculated Results:** Measured force readings compared to calculated (quasi-static) force readings for each motion regime tested. Biologically relevant regimes are highlighted in red. The dashed black line indicates the line of equality. Overall trend indicates a high level of predictability, however over the smaller biologically relevant range, this does not appear to hold true.

**Hypothesis 4: Key parameters used to define the tail motion (i.e. tail amplitude, frequency, etc.), will by themselves, not be able to predict thrust production in any meaningful manner:**

Result: Experimental data supports the hypothesis.

In order to examine whether any key parameters, or combinations thereof could adequately predict thrust production, a multiple linear regression approach was attempted. Unfortunately this failed for two main reasons. Firstly there were relatively few data points, compared the number and range of the variables. While 43 regimes were tested (after they were shown to produce biologically relevant tail tip amplitudes and Strouhal numbers), this was out of a

possible 300 regimes. While the regression did produce a fit for the data, it contained 16 different variables, essentially over predicting the true function.

This problem was compounded by the second issue; co-linearity amongst the various parameters. As was mentioned in the discussion of hypothesis 1, several of the parameters shared some unintended relationships. For example as the pitch angle decreased, the amplitude of motion increased, which in turn caused the frequency to decrease, etc. These relationships were caused by the parameters being related to each other via other intermediate variables (i.e. Strouhal number, tail tip amplitude, etc.). Due to these unintended relationships (and the resulting cause/effect issues inherent in them) combined with the relatively small sample size, the results produced by the multiple regression were not deemed usable.

Instead, a more basic approach was adopted by fitting a linear regression between each key parameter (as well as some intermediate ones) and the measured force (Table 3).

Parameter	ANOVA P Value	$R^2$
Yaw Amplitude, $A_o$	<0.001	0.798
Frequency, $f$	0.584	0.007
Nominal Pitch Angle, $\theta_o$	<0.001	0.849
Phase Lag $\phi$	0.044	0.095
Mean Angle of Attack $\alpha_m$	<0.001	0.353
Tip Strouhal Number $St_{Tip}$	0.851	0.001

**Table 3 - Linear Regressions by Parameter:** Summary statistics on the ability of primary and secondary test parameters to predict force generation across all motion regimes tested.

As can be seen in Table 3, only the phase lag ( $\phi$ ), nominal pitch angle ( $\theta_o$ ) and yaw amplitude ( $A_o$ ) pass an ANOVA test indicating that they are linearly related to the measured thrust. Of

those, only the nominal pitching angle ( $\theta_o$ ) and the yaw amplitude ( $A_o$ ) provide any meaningful level value of prediction. That being said, even using the strongest relationship available ( $\theta_o$ ), it can be seen in Figure 34, that while a general prediction of the trend can be made, predicting specific values is impossible. Again as stated in Hypothesis 1, while a particular value or range of values for a parameter may be required to generate thrust, it does not guarantee it.

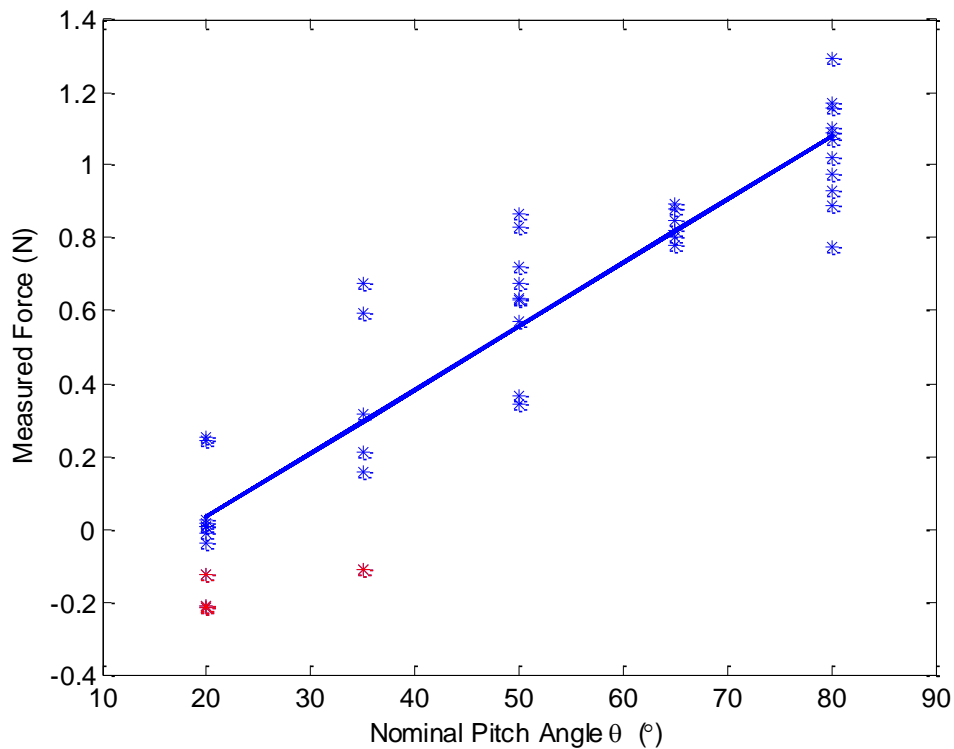


**Figure 34- Force vs  $\theta_o$  Results:** Relationship showing the ability of  $\theta_o$  to predict force generation over all tested motion regimes. Biologically relevant regimes are highlighted in red.

**Hypothesis 5: Secondary, ‘non-standard’ thrust generation mechanisms are possibly contributing to overall thrust production.**

Result: Experimental data does not support the hypothesis.

Over the past several years, experimental analysis of heaving and pitching biological foils has found a number of unexpected lift and thrust generation mechanisms. For example, Dickinson et

al. (1999), found drosophila use high angles of attack for extremely short durations in order to get additional lift by generating momentary stall. They then flip their wings over in order to catch the shed vortex creating still more lift. Vidler et al. (2004), found swifts also use high angles of attack in a similar manner upon landing. As experimental analysis of biologically inspired foils has grown, so to have the number of these 'non-standard' mechanisms discovered.

It was therefore expected that there may be some unaccounted for phenomena which would help explain the unique performance capabilities of these foils as seen in the literature. While due to the fact that no flow visualization data was collected, it seemed unlikely that such phenomena could be identified. However, through a combination of mean force readings and the creation of standardized flow profiles, it was hoped that their existence could be verified. Unfortunately there is little evidence to support this hypothesis, and in fact two major indicators suggest this is not true.

Firstly, it appears that while under-predicting thrust production, the quasi-static analysis did produce a linear relationship with the true forces measured (this is despite the fact that quasi-static analysis would not be able to predict these phenomena). This would indicate (as these phenomena are likely highly dependent on the particular motion regimes) that if they were in fact present and active, this relationship should not be linear.

Furthermore, none of the true force profiles measured for the biologically relevant regimes (Figure 29) showed any major sign of deviation from the quasi-static force profiles (apart from differences in magnitude). This is especially true after correction for symmetry (Figure 31). If these phenomena were present, they would likely create symmetrical and regular unexpected force readings in the profile, much like they did for Dickinson et al. (1999, as seen in Figure 35). It should be noted however, that this is not totally unexpected as drosophila do not use sinusoidal

motions in flapping their wings, making these ‘non-standard’ thrust generation mechanisms much more likely.

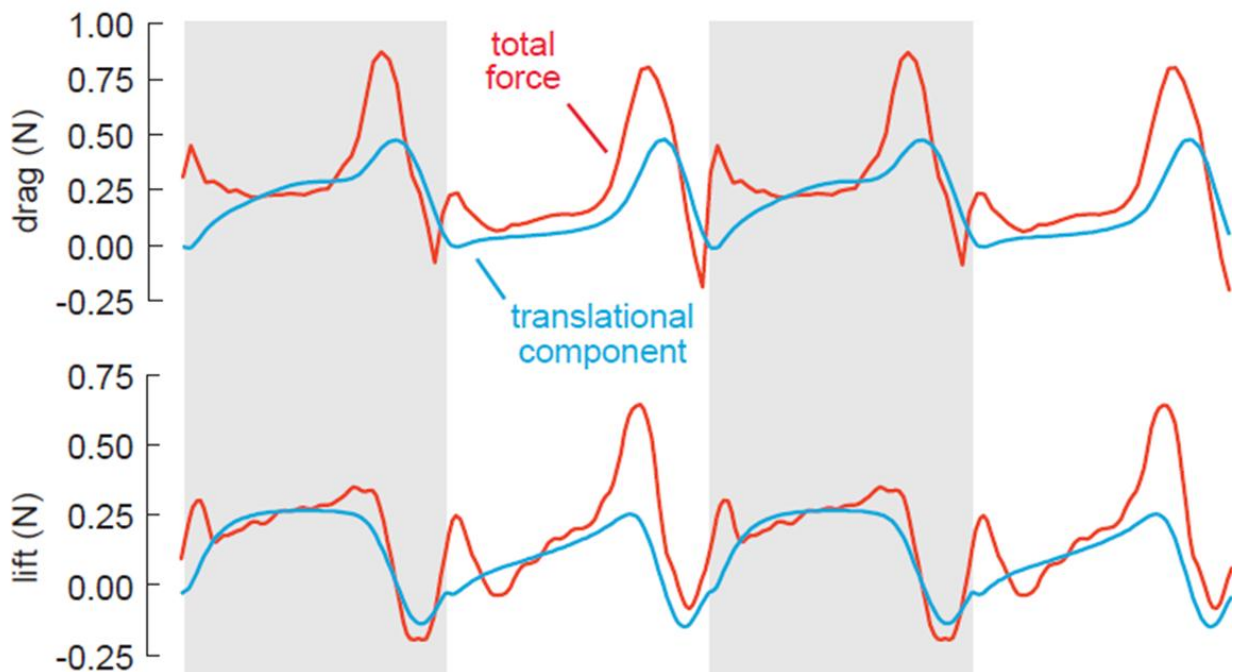


**Figure 35- Drosophila Force Generation:** Thrust and drag values generated by a drosophila, comparing expected transitional forces and total forces. Unexpected peaks indicate presence of ‘non-standard’ lift mechanisms (Figure modified from Dickinson et al., 1999).

There are however two major caveats to conclusion. Firstly there is the matter of the differences of magnitude between the measured and quasi-static force readings. While this is assumed to be due to the fact that quasi-static analysis does not take into account inertial forces, there may be some component of this difference due to unexpected phenomena. The fact that these phenomena would have to be occurring at the exact moment where quasi-static analysis predicts peak thrust in order to avoid detection in the force profiles seems extremely unlikely, but possible. The second caveat is the very real possibility that motion regimes that could generate these phenomena simply were not tested in this study and could be discovered using a more refined range of motion regimes.

**Hypothesis 6: Calculated efficiency (disregarding torsional input) could reach above 90% and possibly even above 100%.**

Results: Experimental data does not support the hypothesis.

The most surprising result in this study was the unexpectedly low efficiency levels measured. Even without accounting for torsional force, the peak efficiency recorded was only at approximately 35%. If torsional forces were included, this value would drop still further. This seems contradictory to both the experimental (Triantafyllou and Triantafyllou, 1995; Anderson et al., 1998) and theoretical evidence (Fish, 1998) already in the literature. There are however several possible explanations for this discrepancy:

- 1) As mentioned in the discussion of hypothesis 2 and 5, there is a very likely possibility that the peak performance regimes of the model tail simply were not tested in the course of this study. More refined testing could easily lead to the discovery of both higher thrust coefficients and efficiency values in line with the literature.
- 2) Furthermore, as stated in the discussion of Hypothesis 1, previous experimental work has often diverged significantly from its biological basis. As such, true biological foils may differ significantly from their idealized experimental counterparts.
- 3) Similarly, theoretical modeling is often conducted using idealized assumptions. While there exists a whole suite of different types of modeling parameters, they all make assumptions of some sort. Whether it be related to aspect ratio, sweep-back angles, infinite spans, or small amplitudes of motion, some assumptions must always be made, and they are never ideal. While investigating the variations amongst these models would be an interesting point of study (see Future Directions), for now it should simply be noted that not all theoretical thunniform modeling is appropriate in all cases. For example Fish

(1998 and 2006) showed that cetaceans have extremely high performance capabilities. This was done using a Chopra's 1977 three dimensional lifting surface approach (Chopra and Kambe, 1977), which assumes an aspect ratio of under 6. While this applies to cetaceans, it does not apply to a whole host of other thunniform swimmers such as most tuna (albacore, bluefin, yellowfin, skipjack), pacific bonito, wahoo, frigate mackerel and many more. A comparison with Fish's results and the data collected in this study are shown in Figure 36.

- 4) Finally, there is the very real possibility that aquatic organisms do not swim at their peak possible performance. There may be unaccounted for tradeoffs that make such behavior either physiologically or environmentally undesirable. As the purpose of this study was to imitate the real life performance of a skipjack tuna, it is possible, that this organism simply operates using different performance characteristics than would be expected.

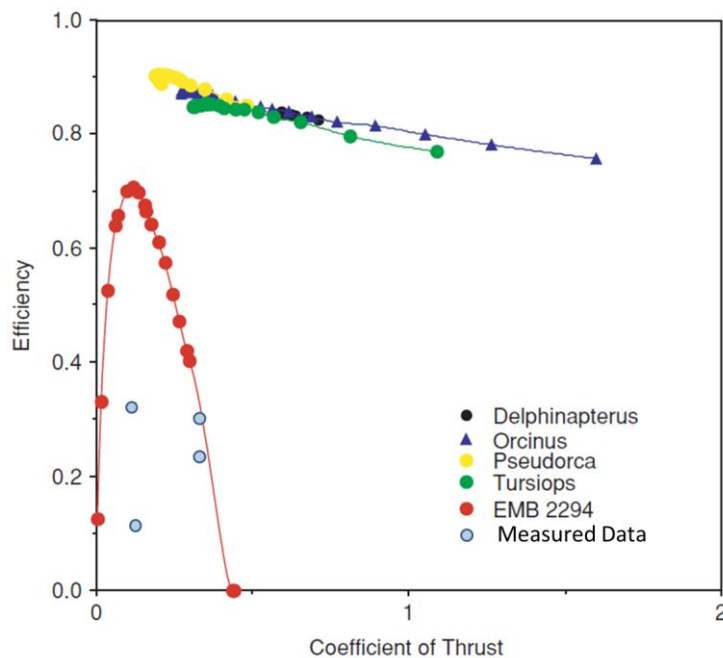


**Figure 36- Performance Comparison:** Comparison of collected data (blue circles) with literature values. Cetacean data was calculated using Chopra's lifting surface approach and compared to a standard propeller (EMB 2294) (Figure modified Fish, 2006).

## **Future Directions**

### **Refined Motion Regimes**

One major outcome of this research was to highlight what ranges of each parameter can (or more importantly can not) produce thrust. Currently only about 10% of the tested regimes proved to be biologically relevant. This makes it extremely difficult to analyze data and determine trends. Therefore the next logical step would be to further refine the motion parameters being tested. Ideally by removing those ranges of the parameters that are known not to generate thrust and concentrating on those that do, a great deal more biologically relevant information can be gained. A possible set of test ranges which according to this research would likely produce a higher number of thrust producing regimes are shown in Table 4.

<b>Parameter</b>	<b>Possible Test Range</b>
Phase Lag $\phi$	60, 70, 80, 90, 100
Nominal Pitch Angle, $\theta_o$	10, 20, 30, 40
Yaw Amplitude, $A_o$	40, 50, 60, 70
Frequency, $f$	TBD by Strouhal Number and Velocity Relationships.

**Table 4 - Recommended Test Parameter Ranges:** Test parameter ranges recommended for future testing.

Obviously similar steps would need to be taken in the new study to ensure that each regime tested correlates with observational data in the literature. However, even with that in mind, these new ranges could easily produce ten times as many biologically relevant test regimes. Ideally this new data set would shed light on some of the questions raised by the current research. Primarily it could help determine peak thrust and efficiency operating parameters for the current foil.

### Theoretical Modeling Comparison

As was mentioned several times in this study, there are numerous theoretical models dedicated to predicting thunniform swimming performance. Generally they are quite complicated and require a detailed knowledge of theoretical fluid modeling. It is interesting to note however that a detailed comparison of the various models and their results on a singular case study has never been done. Once a full set of data describing biologically relevant flow regimes for the skipjack tuna is collected, it would be very interesting to see how these various models compare not only to themselves but to the experimentally collected data.

### Upgrading 'Da Bruce

A key component to any future work using the current apparatus would be upgrading 'Da Bruce' to address minor issues encountered during testing and to increase the reliability of the results.

A list of recommended upgrades are as follows:

- 1) **Replace Cams with Scotch Yokes:** As discussed in the methods and analysis sections, the use of cams did introduce a small measure of error into the sinusoidal motion of the tail. While this was determined to be minimal, it could easily be addressed by switching over to a series of scotch yokes to generate the amplitude and pitching motions.
- 2) **Decrease Gear Ratio Between Rack and Pinion:** The primary purpose of this change would be to allow for a more accurate setting of the pitch angle ( $\theta_o$ ), at the cost of reducing its range. As there no longer appears to be a need to conduct testing of  $\theta_o$  over  $40^\circ$ , this would be an appropriate tradeoff.
- 3) **Increase Reduction on the Motor:** As the higher end of the operating range of the motor was never used, this minor change would allow for easier and more accurate control of the frequency. It would also provide additional torque to the scotch yokes if necessary.

- 4) **Install torque gage:** While this upgrade could prove technically difficult to achieve, if at all possible a torque gauge (or several) should be mounted onto the shaft. This would provide the necessary data to calculate a true value for the efficiency of the foil at any given setting. The main obstacle with this is that the gauges (and associated wiring) will need to be mounted onto a spinning object. However with the reduced ranges of pitch angles to be tested, it may now be possible.
- 5) **Replace the Current Connecting Method Between the Fin and Shaft:** There are many ways of accomplishing this, but possibly the best solution would be to embed a slender pin into the tail model, which could then attach to the shaft above the mirror plane. If possible, this new design would incorporate a method of more accurately resetting the pitch angle to zero between runs. As an added benefit, this would also allow for the reduction in the size of the gap in the mirror plane.
- 6) **Place a Locking Mechanism on the Mirror Plane:** One of the most common issues during testing was the difficulty in properly placing the mirror plane so as not to interfere with the shaft. This could be addressed by simply determining the correct position for the mirror plane and placing a locking mechanism there to ensure proper placement in the future.
- 7) **Increase Spring Constant of Flexible Drive Shaft:** While the flexible shaft is supposed to be essentially non-deformable under torque, it does possess some give. While this likely did not impact testing (as the torque was always applied in a single direction and was more or less constant), it did make setup between runs difficult. Therefore it would be recommended that the spring constant of the shaft be increased. The most straight forward way of doing this would likely be use solid mechanical linkages (i.e. additional gearing) to limit the length of the shaft and to increase its diameter.

8) **Determine a More Suitable Way of Changing Phase Lag:** Changing phase lag was rather tricky with the current apparatus as it required changing the orientation of a small brass coupling attached to a shaft via a small set-screw. Simply increasing the relative size of all the associated parts in this case would likely save a great deal of time and effort in future testing.

### Testing Different Foils

While thunniform propulsion is generally considered to be a singular phenomenon, it is very important to remember that it is widespread across many unrelated species. There is therefore a great deal of variability not only in the motion regimes, but also the caudal tail structures involved. Currently the same explanation is used to describe the propulsion of anything from a 70 ton fin whale to a 7 pound tuna. Examining this variability and its effect on performance in greater detail could prove extremely insightful.

Making models tails from various other species and comparing their performance to that of a skipjack would not be overly difficult given the current apparatus. Motion regimes could be set to those seen in skipjack, the new model species or some intermediate. Moreover even non-thunniform caudal fins, such as those from salmonids, could be tested to examine the effect of the 'standard' thunniform tail on performance. The possibilities in such comparisons are virtually endless and could provide a great deal of new data on the comparative physiology associated with thunniform swimmers.

## Testing Assumptions

Finally, a thorough examination of the assumptions made in this study should be investigated:

- 1) **Sinusoidal Motion of Yaw and Pitching Angle:** While it is generally accepted that the motion of the tail and its pitching angle are roughly sinusoidal, this should be experimentally validated. Kinematic data of this nature could be obtained with the use of high speed cameras. Care however should be taken to ensure that the experimental setup (such as use of a water tunnel) does not compromise the validity of the results.
- 2) **Effect of Chemical Treatment on Caudal Fin Material Properties:** In comparing the mechanical properties of the tail model with the fixed specimen, it was assumed that the chemical treatment of the specimen did not affect its material properties. This assumption should be validated, and can be done so quite easily by comparing the mechanical properties of a tail both before and after chemical treatment.
- 3) **Passive Nature of the Caudal Fin:** Along with the kinematic data obtained in determining the motion of the caudal fin, data could also be collected to help determine if the fin is passive or not. This would be quite technically difficult as it would require the differentiation of tail deformation due to active muscle contraction and passive external forces. However, similar work has been done in the past on mackerel (Gibb et al., 1999), and could possibly be replicated with tuna.

## Conclusion

On the whole this study proved to be quite successful in its goal of recreating thunniform propulsion with a high level of bio-fidelity. Motion parameters, material properties as well as hydrofoil size and shape were all accurately matched to in vivo values. The accuracy of this modeling was confirmed by the apparatus' ability to produce thrust at a level as predicted by whole body drag analysis of the test organism.

Efficiency levels were determined to be surprisingly low when compared to expected literature values. This could have been for a number of reasons, including the possibility that the combination of motion parameters required to produce higher efficiency values simply were not tested in the course of this study. However these results do support research conducted by Sepulveda et al. (2003), which suggested that skipjack tuna have similar cost of transport values to comparable carangiform swimmers. These combined results may indicate that perhaps not all thunniform swimmers operate at the extremely high efficiencies commonly believed. This implies the need for more comparative analysis (in vivo, in vitro and mathematical) on the differences between various types of thunniform swimmers, as to date, they have generally been treated as a single group.

The research conducted thus far opens the door to a great deal of possible future work using similar setup and analysis methods. The most relevant and directly related approach would further refine the motion parameters tested in an effort to confirm or disprove the high efficiency values typically associated with thunniform propulsion.

## **References**

- Anderson, J., Streitlien, K., Barrett, D., & Triantafyllou, M. S. (1998). Oscillating foils of high propulsive efficiency. *Journal of Fluid Mechanics*, 360, 41-72.
- Blake, R. W. (1983). *Fish Locomotion*. Cambridge: Cambridge University Press.
- Blickhan, R., & Cheng, J. (1994). Energy-storage by elastic mechanisms in the tail of large swimmers - A reevaluation. *Journal of Theoretical Biology*, 168(3), 315-321.
- Bose, N., & Lien, J. (1989). Propulsion Of A Fin Whale (Balaenoptera-Physalus) - Why the fin whale is a fast swimmer. *Proceedings of the Royal Society of London B*, 237(1287), 175-200.
- Brill, R. W., & Bushnell, P. G. (2001). The cardiovascular system of tunas. In B. Barbara & E. Stevens (Eds.), *Fish Physiology* (Vol. Volume 19, pp. 79-120): Academic Press.
- Cheng, H., & Murillo, L. (1984). Lunate-tail swimming propulsion as a problem of curved lifting line in unsteady-flow .1. Asymptotic theory. *Journal of Fluid Mechanics*, 143(June), 327-350.
- Chong, C. W., Zhong, Y., Zhou, C. L., Low, K. H., L, G. S. G., & Lim, H. B. (2009). Can the swimming thrust of BCF biomimetics fish be enhanced? *Proceedings of the 2008 IEEE*.
- Chopra, M. (1974). Hydromechanics of lunate-tail swimming propulsion. *Journal of Fluid Mechanics*, 64, 375-391.
- Chopra, M., & Kambe, T. (1977). Hydromechanics of lunate-tail swimming propulsion. Part 2. *Journal of Fluid Mechanics*, 79, 49-69.
- Dickinson, M., Lehmann, F.-O., & Sane, S. (1999). Wing rotation and the aerodynamic basis of insect flight. *Science, New Series*, 284(5422), 1954-1960.
- Fierstine, H. L., & Walters, V. (1968). *Studies in locomotion and anatomy of scombroid fishes* (Vol. 6). Los Angeles: Southern California Academy of Sciences.
- Fish, F. E. (1996). Transitions from drag-based to lift-based propulsion in mammalian swimming. *American Zoologist*, 36(6), 628-641.
- Fish, F. E. (1998). Comparative kinematics and hydrodynamics of odontocete cetaceans: morphological and ecological correlates with swimming performance. *Journal of Experimental Biology*, 201(20), 2867.
- Fish, F. E. (2006). Limits of nature and advances of technology: What does biomimetics have to offer to aquatic robots? *Applied Bionics and Biomechanics*, 3(1), 49-60.

- Gibb, A. C., Dickson, K. A., & Lauder, G. V. (1999). Tail kinematics of the chub mackerel *Scomber japonicus*: testing the homocercal tail model of fish propulsion. *Journal of Experimental Biology*, 202(18), 2433-2447.
- Klingener, F. (Contributor). (April, 2011). Comparing simple crank/slider and scotch yoke mechanisms. *Wolfram Demonstrations Project*. Retrieved from <http://demonstrations.wolfram.com/ComparingSimpleCrankSliderAndScotchYokeMechanisms/>
- Knower, T., Shadwick, R., Katz, S., Graham, J., & Wardle, C. (1999). Red muscle activation patterns in yellowfin (*Thunnus albacares*) and skipjack (*Katsuwonus pelamis*) tunas during steady swimming. *Journal of Experimental Biology*, 202, 2127-2138.
- Lau, T., & Kelso, R. (2007). *The forces on a fish-inspired unsteady hydrofoil*. Paper presented at the 16th Australasian Fluid Mechanics Conference Gold Coast, Queensland Australia.
- Lau, T., Kelso, R., & Hassan, E. (2004). *Flow visualisation of a pitching and heaving hydrofoil*. Paper presented at the 15th Australasian Fluid Mechanics Conference, University of Sydney.
- Lauder, G. V., Anderson, E. J., Tangorra, J., & Madden, P. G. A. (2007). Fish biorobotics: kinematics and hydrodynamics of self-propulsion. *Journal of Experimental Biology*, 210(16), 2767.
- Lauder, G. V., & Madden, P. G. A. (2006). Learning from fish: kinematics and experimental hydrodynamics for roboticists. *International Journal of Automation and Computing*, 4, 325-335.
- Lauder, G. V., & Tytell, E. D. (2005). Hydrodynamics of undulatory propulsion. *Fish Physiology*, 23, 425-468. Academic Press.
- Lighthill, M. (1969). Hydromechanics of aquatic animal propulsion. *Annual Review of Fluid Mechanics*, 1, 413-446.
- Lighthill, M. (1970). Aquatic animal propulsion of high hydromechanical efficiency. *Journal of Fluid Mechanics*, 44, 265-301.
- Lindsey, C. C. (1978). Form, function and locomotory habits in fish. *Fish Physiology*, 8, 1-100. Academic Press.
- Liu, P., & Bose, N. (1993). Propulsive performance of 3 naturally-occurring oscillating propeller planforms. *Ocean Engineering*, 20(1), 57-75.
- Magnuson, J. (1979). Locomotion by scombrid fishes: Hydromechanics, morphology, and behavior. *Fish Physiology*, 7, 239-313.
- Parry, D. A. (1949). The swimming of whales and a discussion of gray's paradox. *Journal of Experimental Biology*, 26(1), 24-28.

- Sepulveda, C. A., Dickson, K. A., & Graham, J. B. (2003). Swimming performance studies on the eastern Pacific bonito *Sarda chiliensis*, a close relative of the tunas (family Scombridae) I. Energetics. *Journal of Experimental Biology*, 206(16), 2739-2748.
- Sfakiotakis, M., Lane, D., & Davies, J. (1999). Review of fish swimming modes for aquatic locomotion. *IEEE Journal of Oceanic Engineering*, 24(2), 237-252.
- Shadwick, R. (2005). How tunas and Lamnid sharks swim: An evolutionary convergence. *American Scientist*, 93(6), 524-531.
- Triantafyllou, G. S., Triantafyllou, M. S., & Grosenbaugh, M. (1993). Optimal thrust development in oscillating foils with application to fish propulsion. *Journal of Fluids and Structures*, 7(2), 205-224.
- Triantafyllou, M., Triantafyllou, G., & Yue, D. (2000). Hydrodynamics of fishlike swimming. *Annual Review of Fluid Mechanics*, 32, 33-53.
- Triantafyllou, M. S., Techet, A., Zhu, Q., Beal, D., Hover, F., & Yue, D. (2002). Vorticity control in fish-like propulsion and maneuvering. *Integrative and Comparative Biology*, 42(5), 1026
- Triantafyllou, M. S., & Triantafyllou, G. S. (1995). An efficient swimming machine. *Scientific American*, 272(3), 64-71.
- Videler, J., Stamhuis, E., & Povel, G. (2004). Leading-edge vortex lifts swifts. *Science*, 306(5703), 1960.
- Webb, P. (1975). *Hydrodynamics and Energetics of Fish Propulsion* (Vol. 190). Ottawa.
- Westneat, M. W., Hoese, W., Pell, C. A., & Wainwright, S. A. (1993). The horizontal septum: Mechanisms of force transfer in locomotion of scombrid fishes (Scombridae, Perciformes). *Journal of Morphology*, 217(2), 183-204.
- Westneat, M. W., & Wainwright, S. A. (2001). 7. Mechanical design for swimming: muscle, tendon, and bone. In B. Barbara & E. Stevens (Eds.), *Fish Physiology* (Vol. Volume 19, pp. 271-311): Academic Press.
- Yuen, H. S. H. (1966). Swimming Speeds of Yellowfin and Skipjack Tuna. *Transactions of the American Fisheries Society*, 95(2), 203 - 209.

## **Appendix A- Model Creation Instructions**

- 1) Mix together enough Tropicalgin to cover an entire half specimen (up to peduncle), as per manufactures instructions.
- 2) While keeping a small piece of doweling at the tip of the tail, place the specimen between two layers of Tropicalgin. It is important to ensure the doweling runs from the inside of the cast to the outside as the hole it creates is needed to prevent the air bubbles forming during the molding stage.
- 3) Allow the Tropicalgin to set as per manufacturer's instructions. Carefully remove specimen and doweling, ensuring not to damage the cast. Let cast sit for approximately one hour to allow for any moisture inside the cast to dissipate.
- 4) Mix together enough Flexacryl Hard to create tail model. Turn cast upright and pour the mixture into the hole created by the peduncle. Allow to set for several hours before breaking away the cast to reveal the mould.
- 5) Using a band saw, roughly level the peduncle end of the model along the axis of cemetery. Use a file to remove any other inconsistencies such as the plug generated at the doweling hole.
- 6) Determine the axis of rotation along the peduncle end of the model and super glue a small nut at this point. This nut will be used to attach the tail to the test apparatus.

## **Appendix B- Boundary Layer Calculations**

First the Reynolds number of the system is calculated:

$$Re = \frac{lU}{\nu}$$

Where  $l$  is the characteristic length (in this case the distance to the test section),  $U$  is the water velocity, and  $\nu$  is the kinematic viscosity of the water:

$$Re = \frac{(0.4m)(1.0m/s)}{1.156 \times 10^{-6} m^2/s} = 3.46 \times 10^5$$

If laminar, boundary layer ( $\delta$ ) is:

$$\delta = \frac{l(5)}{Re^{1/2}} = \frac{0.4(5)}{(3.46 \times 10^5)^{1/2}} = 3.4mm$$

If turbulent, boundary layer ( $\delta$ ) is:

$$\delta = \frac{l(0.16)}{Re^{1/7}} = \frac{0.4(0.16)}{(3.46 \times 10^5)^{1/7}} = 10mm$$

## Appendix C- Detailed Results

Motion Regime	Frequency $f$ (Hz)	Phase Lag $\phi$ ( $^{\circ}$ )	Nominal Pitch Angle $\theta$ ( $^{\circ}$ )	Yaw Amplitude $A_o$ (mm)	Measured Thrust (N)	Calculated Thrust (N)
1	2.4	0	20	45	-0.037	0.147
2	2.4	0	35	45	0.595	0.263
3	2.4	0	50	30	0.830	0.439
4	2.4	0	65	30	0.895	0.550
5	2.4	0	80	15	1.089	0.629
6	2.4	20	20	45	0.252	0.080
7	2.4	20	35	45	0.677	0.228
8	2.4	20	50	30	0.673	0.390
9	2.4	20	65	30	0.879	0.504
10	2.4	20	80	15	0.973	0.637
11	2.4	20	80	30	0.775	0.645
12	2.4	40	20	45	0.016	0.011
13	2.4	40	20	60	0.026	-0.016
14	2.4	40	35	45	0.314	0.153
15	2.4	40	50	30	0.635	0.395
16	2.4	40	65	30	0.800	0.536
17	2.4	40	80	30	0.886	0.631
18	2.4	60	20	60	-0.125	-0.116
19	2.4	60	35	45	0.210	0.080
20	2.4	60	50	45	0.568	0.329
21	2.4	60	65	30	0.821	0.549
22	2.4	60	80	30	0.931	0.666
23	2.4	80	20	60	-0.214	-0.157
24	2.4	80	35	60	-0.111	-0.160
25	2.4	80	50	45	0.364	0.358
26	2.4	80	65	45	0.781	0.548
27	2.4	80	80	30	1.100	0.667
28	2.7	0	20	45	-0.010	0.150
29	2.7	0	50	30	0.864	0.439
30	2.7	0	80	15	1.293	0.630
31	2.7	20	20	45	0.243	0.076
32	2.7	20	50	30	0.723	0.387
33	2.7	20	80	15	1.023	0.639
34	2.7	40	20	45	0.008	0.001
35	2.7	40	50	30	0.632	0.389
36	2.7	60	35	45	0.158	0.048
37	2.7	60	65	30	0.848	0.548
38	2.7	80	20	60	-0.213	-0.182
39	2.7	80	50	45	0.343	0.342
40	2.7	80	80	30	1.156	0.678
41	3	0	80	15	1.172	0.632
42	3	20	80	15	1.071	0.640
43	3	40	20	45	0.005	-0.010